ADJOINT BASED OPTIMIZATION OF SUPERSONIC CONVERGING
DIVERGING NOZZLE

A THESIS SUBMITTED TO
THE GRADUATE SCHOOL OF NATURAL AND APPLIED SCIENCES
OF
MIDDLE EAST TECHNICAL UNIVERSITY

BY

BERKAN YERLİKAYA

IN PARTIAL FULFILLMENT OF THE REQUIREMENTS
FOR
THE DEGREE OF MASTER OF SCIENCE
IN
AEROSPACE ENGINEERING

SEPTEMBER 2019

Approval of the thesis:

ADJOINT BASED OPTIMIZATION OF SUPERSONIC CONVERGING DIVERGING NOZZLE

submitted by **BERKAN YERLİKAYA** in partial fulfillment of the requirements for the degree of **Master of Science in Aerospace Engineering Department, Middle East Technical University** by,

Prof. Dr. Halil Kalıpçılar
Dean, Graduate School of **Natural and Applied Sciences**   _____

Prof. Dr. İsmail Hakkı Tuncer
Head of Department, **Aerospace Engineering**   _____

Prof. Dr. İsmail Hakkı Tuncer
Supervisor, **Aerospace Engineering, METU**   _____

Examining Committee Members:

Prof. Dr. Yusuf Özyörük
Aerospace Engineering, METU   _____

Prof. Dr. İsmail Hakkı Tuncer
Aerospace Engineering, METU   _____

Prof. Dr. Hüseyin Nafiz Alemdaroğlu
School of Civil Aviation, Atilim University   _____

Assoc. Prof. Dr. Sinan Eyi
Aerospace Engineering, METU   _____

Assoc. Prof. Dr. Utku Kânoğlu
Aerospace Engineering, METU   _____

Date: 10.09.2019

I hereby declare that all information in this document has been obtained and presented in accordance with academic rules and ethical conduct. I also declare that, as required by these rules and conduct, I have fully cited and referenced all material and results that are not original to this work.

Name, Surname: Berkan, Yerlikaya

Signature   :

ABSTRACT

ADJOINT BASED OPTIMIZATION OF SUPERSONIC CONVERGING DIVERGING NOZZLE

Yerlikaya, Berkan
Master of Science, Aerospace Engineering
Supervisor: Prof. Dr. İsmail Hakkı Tuncer

September 2019, 80 pages

The nozzle produces the required thrust for the vehicle in an aircraft or rocket engine by expanding and accelerating the exhaust gas. In this study, the thrust of a supersonic converging-diverging nozzle is optimized by using SU2 software and the adjoint-based optimization tool. During the design optimization procedure, the inlet area, the exit area and the length of the nozzle are kept constant. The main objective is to obtain the maximum thrust within the geometric limitations. In order to maximize the thrust, the exit Mach number and the mass flow rate are selected as the objective functions. They are employed individually and in an equally weighted combination. The highest value in terms of thrust is achieved at the end of the unconstrained multi objective optimization study with low total pressure at the exit of the nozzle. Therefore, a total pressure value is assigned as a constraint to the multi objective optimization. Finally, thrust value is increased with establishing the desired total pressure recovery.

Keywords: CFD, Design Optimization, Nozzle, Compressible Flows

ÖZ

ADJOİNT TABANLI SESÜSTÜ YAKINSAK IRAKSAK LÜLE OPTİMİZASYONU

Yerlikaya, Berkan
Yüksek Lisans, Havacılık ve Uzay Mühendisliği
Tez Danışmanı: Prof. Dr. İsmail Hakkı Tuncer

Eylül 2019, 80 sayfa

Bir uçak veya roket motorunda lüle, egzoz gazını genişleterek ve ivmelendirerek araç için gerekli itkiyi üretir. Bu çalışmada, süpersonik yakınsak-ıraksak bir lülenin itkisi SU2 yazılımı ve eklenik (İng. adjoint) tabanlı optimizasyon aracı kullanılarak optimize edilmiştir. Tasarım optimizasyonu sırasında, lülenin giriş-çıkış alanları ve uzunluğu sabit tutulmuştur. Asıl amaç, geometrik sınırlamalar içinde maksimum itkiyi elde etmektir. İtkiyi en üst seviyeye çıkarmak için lüle çıkışındaki Mach sayısı ve kütle debisi optimizasyonun amaç fonksiyonları olarak seçilmiştir. Optimizasyonlar, bu amaç fonksiyonlarının ayrı ayrı ve birlikte eşit ağırlıkla kullanılması ile gerçekleştirilmiştir. İtki açısından en yüksek değer sınırlandırılmamış çok amaçlı optimizasyon sonucunda toplam basınçta kayıp yaşanarak elde edilmiştir. Bu nedenle toplam basınç çok amaçlı optimizasyona bir sınırlayıcı olarak atanmıştır. Sonuç olarak, optimizasyon aracı itki değerini istenen basınç geri kazanımıyla sağlamayı başarmıştır.

Anahtar Kelimeler: HAD, Tasarım Optimizasyonu, Lüle, Sıkıştırılabilir Akışlar

To my family

ACKNOWLEDGEMENTS

TABLE OF CONTENTS

LIST OF TABLES

TABLES

LIST OF FIGURES

FIGURES

LIST OF ABBREVIATIONS

ABBREVIATIONS

AD	Algorithmic Differentiation
ADL	Aerospace Design Laboratory
BSL	Baseline
CFD	Computational Fluid Dynamics
FDM	Finite Difference Method
FEM	Finite Element Method
FFD	Free Form Deformation
FVM	Finite Volume Method
JST	Jameson Schmidt Turkel
NSE	Navier Stokes Equation
PDE	Partial Differential Equations
RANS	Reynolds Averaged Navier Stokes
SA	Spalart Allmaras
SST	Shear Stress Transport
SU^2	Stanford University Unstructured

CHAPTER 1

INTRODUCTION

Nozzle is the last but not the least important part of a propulsion system. For all aerospace applications a propulsion system must be capable of generating thrust that is needed for an operation condition. Required thrust is generated by converting internal energy of working fluid into kinetic energy. Accordingly, nozzles are designed in order to obtain optimum kinetic energy from combustion products of a propulsion system. This is achieved by accelerating the working fluid with area change through nozzle profile. As the high pressure and high temperature flow is accelerated, net thrust is obtained from that medium.

1.1. Supersonic Converging Diverging Nozzle Concept

In this study, supersonic converging diverging nozzles are investigated. Supersonic converging diverging nozzles are used in aerospace applications that are used for high speed operating regimes. These nozzles are also called de Laval Nozzle. For the ideal condition, the converging part of nozzle has subsonic flow inside of it. Accordingly, in the diverging part flow accelerates to supersonic regime. This is necessary for obtaining optimum thrust. However, there are other conditions that reduce the net thrust generated by converging diverging nozzle. [1] As an example, subsonic flow tries to expand due to area change across the nozzle however it reaches the maximum Mach number at throat section and exits the nozzle again with subsonic flow. As another example, when the ambient pressure is above the exit pressure flow undergoes sudden compression. This phenomenon is called overexpansion and reduces the net thrust. The net thrust obtained from a nozzle is expressed with Equation 1.1.

$$
\begin{aligned}
Thrust &= (Mass\ Flow\ Rate)x(Nozzle\ Exit\ Velocity) \\
&\quad + (\ Nozzle\ Exit\ Pressure \\
&\quad - Ambient\ Pressure)x(Nozzle\ Exit\ Area)
\end{aligned}
\tag{1.1}
$$

As it can be seen from Equation 1.1 the generated net thrust depends on mass flow rate, nozzle exit velocity, nozzle exit pressure, ambient pressure and nozzle exit area. There is correlation between each component of the thrust equation. Schematic of a supersonic converging diverging nozzle is represented in the following schematic Figure 1.1.
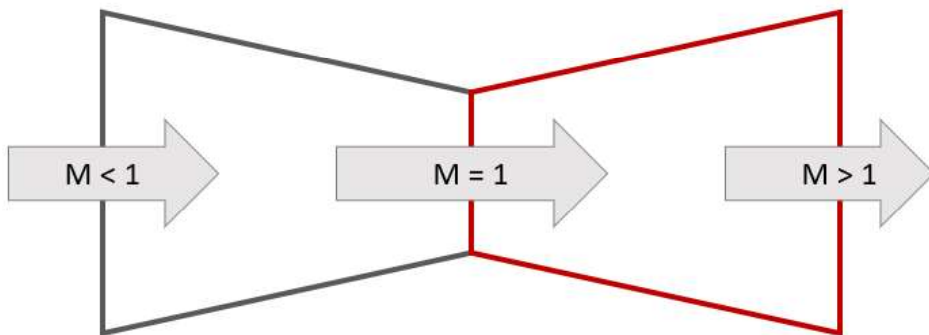
Figure 1.1. Supersonic Converging Diverging Nozzle Example

In the design process nozzle performance parameters must be clarified carefully.[2] For this study main performance parameter is chosen as thrust. To fix the design condition nozzle chamber values are kept constant. In addition, nozzle length, inlet and outlet area of the supersonic converging diverging nozzle are not changed. Therefore, throat and exit angle are subjected to the optimization process in order to obtain optimum thrust for the given conditions.

1.1.1. Supersonic Converging Diverging Nozzle Types

The varying cross-section of supersonic converging diverging nozzle helps flow to convert its internal energy to the kinetic energy in order to produce thrust in a way that keeping uniformity of the fluid velocity as appropriate as possible. For this reason, the contour of a supersonic converging diverging nozzle must be designed in the most efficient way. In terms of their shapes, nozzles are categorized into three; conical, bell and annular types.[3]

a

b

c
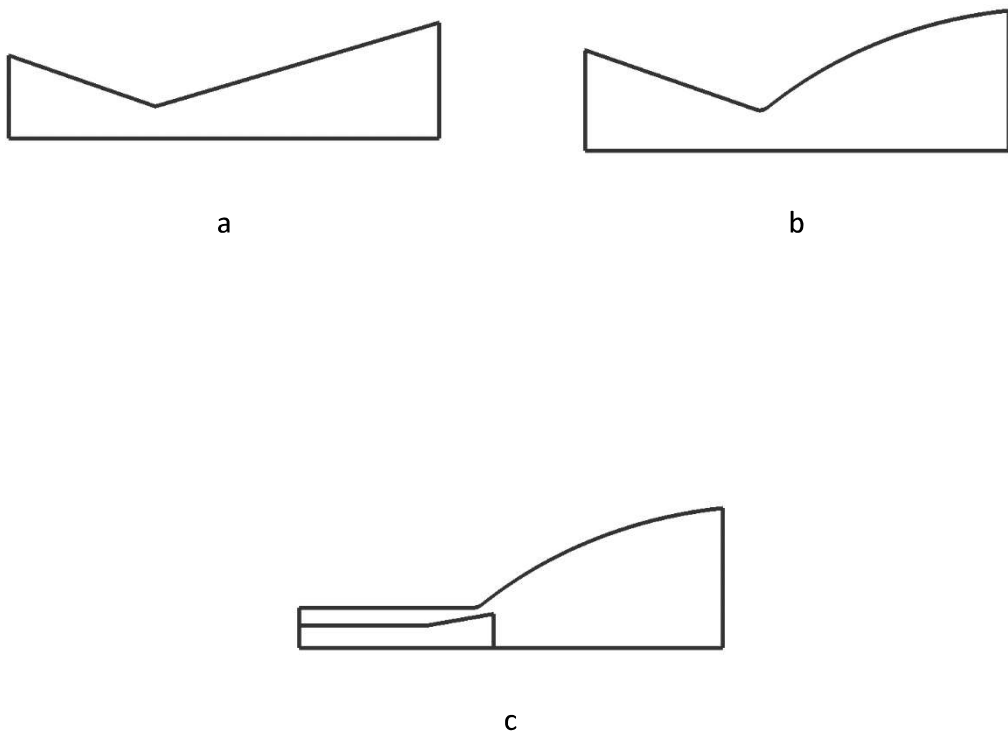
Figure 1.2 a) Conical Nozzle Schematic b) Bell Nozzle Schematic c) Annular Nozzle Schematic

The conical nozzle is the simplest profile to achieve the area ratio needed for a design condition. It basically consists of a divergent part with walls that have constant angle. Due to its simple shape, the conical nozzle concept is the most appropriate one to manufacture among others. However, to produce maximum thrust from a predetermined area ratio divergent angle of a conical nozzle must be kept small for the purpose of having the axial component of exit velocity as much as possible. [3][4]

Unlike conical nozzle concept, bell shape nozzles have varying wall angle through the divergent section. In this model, divergent angle right after the throat is high and tends to decrease until the exit section. The reason behind this is to reduce the length of the nozzle and obtain relatively more uniform flow with respect to conical nozzles. [3][4]

Annular nozzle concept basically consists of a ring shape combustion chamber and a center body inside of it. It is a complex design with respect to other concepts. However, for off-design conditions annular nozzles are suitable for area adjustment accordingly.[3][4]

1.2. Gradient-Based Optimization

Optimization is the task under certain conditions to obtain the best results. The first step in an optimization problem is to define a set of parameters called design variables. Then it is attempted to obtain the best combination of design variables for the maximum gain. It is desirable to complete this process with minimum effort and as soon as possible. Therefore, many techniques for this challenge have been developed. These methods can be classified under two main headings. These are called as gradient-based and gradient-free optimizations. Random search and genetic algorithms are examples of gradient-free optimizations. Although they provide good results for some optimization problems, they become infeasible as design variables increase. Unlike gradient-free optimizations, gradient-based optimizations have an extra information. This information is the gradient of the objective function. By

following the direction of gradient vector, the maximum or minimum point of the objective function can be reached. The adjoint-based optimization, which is used in the current study, is included in the class of gradient-based optimizations. The main advantage of adjoint approach is that it is independent of the number of design variables.

1.3. Stanford University Unstructured

In this study, while supersonic converging diverging nozzles are investigating, Stanford University Unstructured (SU^2) code is used. SU^2 is an open-source PDE based analysis and design tool that is developed by ADL (Aerospace Design Laboratory) Stanford University. The SU^2 platform constructed with C++ language and for the parallelization MPI is used.[5] The code mainly focuses on problems that are investigating flow phenomena defined in RANS equations constructed on unstructured grids. Along with the RANS equations; turbulence models SST and SA are integrated. Thanks to the implementation of adjoint based gradient evaluation, the SU^2 suite becomes an important design tool. Together with design optimization; owing to the adjoint implementation, the tool has capability of statistical analysis like computation of uncertainties and grid adaptation. Therefore, the SU^2 suite is appropriate for multi-disciplinary problems that requires cooperation of different mathematical models.

As mentioned, the high-fidelity open source software suite SU^2 is designed for solving PDE's such as Euler and RANS equations. In order to define a problem, a configuration file is used. The file contains options defining boundary conditions, initial conditions, fluid properties, turbulence models, preferences to obtain converged solution, spatial discretization schemes, time integration choices, geometry parametrization methods, discrete and continuous adjoint approaches and their parameters, design variable definitions and predetermined objective functions. In this study, RANS equations are solved with SU2_CFD module that comes with the software suite. FVM is used with implicit integration scheme in time. For the

geometry parametrization and grid deformation SU2_DEF module is used. By using this module FFD boxes are created and geometry is deformed according to the design variables. A python script is used in order to work flow solution, grid deformation and adjoint solution in harmony. Lastly, to post-process the outputs from the studies SU2_SOL module is employed.[6] [7]

1.4. Literature Survey

Adjoint methods are utilized firstly by Jameson in 1980's for computational fluid dynamics applications. He applied these methods into solution of potential flow and Euler equations. Afterwards, adjoint methods are used for sensitivity analysis and aerodynamic design optimization studies.[8] Besides adjoint methods the very first applications of nozzle optimization procedures consist of different approaches.

Like in the adjoint methods, there are other ways to calculate gradients through a flow field. In 1967, H. L. Rozendaal established a doctoral thesis based on design optimization of rocket nozzles. The aim of the thesis is obtaining optimum thrust by using the steepest descents method. The constraints of thesis are keeping total length of the nozzle, slope of the diverging section and wetted area of the nozzle constant. The author tries to have maximum thrust by establishing all the constraints separately.[9]

Method of characteristics is also a way to design a supersonic converging diverging nozzle geometry. In 1988, A. Haddad published a doctoral thesis about designing non-axisymmetric supersonic nozzles. The main method for obtaining the solution of flow fields is method of characteristics. For both elliptical and wedge like nozzles, optimization studies are applied; the aim was having requested Mach number and nozzle length. The study contains experimental and theoretical work.[10]

In place of adjoint methods, there is another way of finding an optimized value for a performance parameter which is trying different values from the design spice. This method is not as mathematically complex as adjoint method but also does not have to give the best value of the design space. As an example, in 2014, K. S. Patel

6

published a journal paper having study of design optimization of supersonic nozzles by trying different divergent section angles. The whole study is based on computational fluid dynamics and optimization procedure consists of trying different angles for divergent section.[11] Moreover, Swaroopini et. Al. published a study on obtaining higher exit velocity from a baseline geometry. This work is again based on trying different divergent section angles on nozzle geometry.[12]

As mentioned, in this thesis discrete adjoint method is used in order to generate optimum geometry for a supersonic converging diverging nozzle baseline. Like in this work, in 2017 Caramia et. Al. used same gradient calculation method for nozzle optimization. On contrary, the work done by Caramia et. Al. is based on inviscid flow formulation.[13]

1.5. Objectives

The objective of thesis is thrust optimization of a supersonic converging diverging nozzle using adjoint based gradient evaluation. The ultimate thrust optimization goal is planned to achieve by choosing exit Mach number and mass flow rate as an objective function. This can be done by studying on each parameter separately or together. During the design optimization procedure inlet area and the exit area of the nozzle kept constant. The main idea here is obtaining optimum thrust with geometric limitations. Also, there can't be discontinuity in the flow field of optimized geometry. To conclude, it is planned to achieve optimum thrust with choosing Mach number and mass flow rate as objectives, changing nozzle profile while satisfying geometric limitations and having no distortions through the flow field.

1.6. The Scope of Thesis

The thesis mainly focuses on the capabilities of an open source computational fluid dynamics and optimization tool SU^2 on analysis and design of supersonic converging diverging nozzle. Different grids are employed in order to see their effects on the flow solution. Consequences of the free form deformation boxes constructed on the baseline geometry are investigated. Assessment of the design

objectives covers a large area along the study. Effects of Mach number maximization, mass flow rate maximization and multi objective optimization containing Mach number and mass flow rate maximization on the net thrust are examined. Also, a total pressure recovery constraint is applied to the multi objective study. Therefore, the work here establishes the utilization of an open source tool onto design optimization of supersonic converging diverging nozzle. Accordingly, present study gives outputs that says the applicability of SU^2 on compressible flow problems.

CHAPTER 2

METHODOLOGY

The main idea of this study is optimization of a supersonic converging diverging nozzle. This section discribes the govening flow equations and turbulence models. Then, Computational Fluid Dynamics techniques in SU^2, optimization procedure and optimization method is presented in this section.

2.1. Governing Equations

In the first place, flow calculations are done on fluid in macroscopic scale. For supersonic converging diverging nozzle, the flow is considered; viscous and compressible. In addition, molecular interactions are ignored. Therefore, Navier Stokes equations are used in order to take conservation of mass, conservation of momentum and conservation of energy equations into consideration.

Simply conservation of mass equation is defined by balancing the rate of mass change through the control volume with net rate of mass flow into control volume. Accordingly, mass conservation equation is as follows.[14]

$$\frac{\partial \rho}{\partial t} + \frac{\partial (\rho u)}{\partial x} + \frac{\partial (\rho v)}{\partial y} + \frac{\partial (\rho w)}{\partial z} = 0 \tag{2.1}$$

Based on Newton's second law change in momentum is equal to the sum of all the acting forces. Conservation of momentum equation can be drawn by including surface forces and body forces separately. In detail, surface forces are pressure force and viscous force. Examples of body forces can be gravitational force and electromagnetic force. Therefore; x, y and z components of the conservation of momentum equation are given respectively.[14]

9

$$\rho \frac{Du}{Dt} = \frac{\partial(-p + \tau_{xx})}{\partial x} + \frac{\partial(\tau_{yx})}{\partial y} + \frac{\partial(\tau_{zx})}{\partial z} + S_{Mx} = 0$$

$$\rho \frac{Dv}{Dt} = \frac{\partial(\tau_{xy})}{\partial x} + \frac{\partial(-p + \tau_{yy})}{\partial y} + \frac{\partial(\tau_{zy})}{\partial z} + S_{My} = 0 \qquad (2.2)$$

$$\rho \frac{Dw}{Dt} = \frac{\partial(\tau_{xz})}{\partial x} + \frac{\partial(\tau_{yz})}{\partial y} + \frac{\partial(-p + \tau_{zz})}{\partial z} + S_{Mz} = 0$$

According to the first law of thermodynamics, addition of heat transfer to the rate of work done on to the system is equal to the change in energy. Work done by surface forces, energy addition by heat transfer and source term bring forth the conservation of energy equation. Thus, conservation of energy equation can be expressed by using these terms.[14]

$$\rho \frac{DE}{Dt} = -div(\rho \boldsymbol{u})$$

$$+ \left[\frac{\partial(u\tau_{xx})}{\partial x} + \frac{\partial(u\tau_{yx})}{\partial y} + \frac{\partial(u\tau_{zx})}{\partial z} \right.$$

$$+ \frac{\partial(v\tau_{xy})}{\partial x} + \frac{\partial(v\tau_{yy})}{\partial y} + \frac{\partial(v\tau_{zy})}{\partial z} \qquad (2.3)$$

$$+ \frac{\partial(w\tau_{xz})}{\partial x} + \frac{\partial(w\tau_{yz})}{\partial y} + \left. \frac{\partial(w\tau_{zz})}{\partial z} \right]$$

$$+ div(kgradT) + S_E$$

2.2. Turbulence Model

During the study for the verification procedure two different turbulence models are used. The first one is Shear Stress Transport (SST) turbulence model which is a two-equation turbulence model. The second one is a one equation turbulence model called Spalart Allmaras (SA). These models are available in the options of SU^2. They are described in this section briefly.

2.2.1. Spalart Allmaras Turbulence Model

Spalart Allmaras turbulence model is one equation model can be used for structured and unstructured grids easily. This is due to the fact that the equation uses the information at the point where the calculation proceeds. Therefore, it is independent

from other points. Accordingly, this semi-empirical model is applicable for any type of grid and easy to implement. Equations that express the SA turbulence model are as follows.[15][16]

$$\varepsilon_m = \vec{v}_t f_{v_1} \tag{2.4}$$

$$\frac{D\vec{v}_t}{Dt} = c_{b_1}[1 - f_{t_2}]\tilde{S}\vec{v}_t - \left(c_{w_1}f_w - \frac{c_{b_1}}{\kappa^2}f_{t_2}\right)\left(\frac{\vec{v}_t}{d}\right)^2$$
$$+ \frac{1}{\sigma}\frac{\partial}{\partial x_k}\left[(v + \vec{v}_t)\frac{\partial \vec{v}_t}{\partial x_k}\right] + \frac{c_{b_2}}{\sigma}\frac{\partial \vec{v}_t}{\partial x_k}\frac{\partial \vec{v}_t}{\partial x_k} \tag{2.5}$$

Here;

$$c_{b_1} = 0.1355, \quad c_{b_2} = 0.622, \quad c_{v_1} = 7.1, \quad \sigma = 2/3$$
$$c_{w_1} = \frac{c_{b_1}}{\kappa^2} + \frac{1 + c_{b_2}}{\sigma}, \quad c_{w_2} = 0.3, \quad c_{w_3} = 2, \quad \kappa = 0.41$$
$$f_{v_1} = \frac{\chi^3}{\chi^3 + c_{v_1}^3}, \quad f_{v_2} = 1 - \frac{\chi}{1 + \chi f_{v_1}}, \quad f_w = g\left[\frac{1 + c_{w_3}^6}{g^6 + c_{w_3}^6}\right]^{1/6} \tag{2.6}$$
$$\chi = \frac{\vec{v}_l}{v}, \quad g = r + c_{w_2}(r^6 - r), \quad r = \frac{\vec{v}_t}{\tilde{S}\kappa^2 d^2}$$
$$\tilde{S} = S + \frac{\vec{v}_t}{\kappa^2 d^2}f_{v_2}, \quad S = \sqrt{2\Omega_{ij}\Omega_{ij}}$$
$$f_{t_2} = c_{t_3}e^{-c_{t_4}\kappa^2}, \quad c_{t_3} = 1.1, \quad c_{t_4} = 2$$

Vorticity and the distance are defined as S and d tags. In the wall no slip boundary condition is applied to the tangential velocity.

$$\Omega_{ij} = 1/2\left(\frac{\partial u_i}{\partial x_j} - \frac{\partial u_j}{\partial x_i}\right) \tag{2.7}$$

Through the boundary layer equation can be expressed as;

11

$$u\frac{\partial \vec{v}_t}{\partial x} + v\frac{\partial \vec{v}_t}{\partial y} = c_{b_1}(1 - f_{t_2})\tilde{S}\vec{v}_t$$

$$+ \frac{1}{\sigma}\left\{\frac{\partial}{\partial y}\left[(v + \vec{v}_t)\frac{\partial \vec{v}_l}{\partial y}\right] + c_{b_2}\left(\frac{\partial \vec{v}_t}{\partial y}\right)^2\right\} \qquad (2.8)$$

$$- \left(c_{w_1}f_w - \frac{c_{b_1}}{\kappa^2}f_{t_2}\right)\left(\frac{\partial \vec{v}_l}{\partial y}\right)^2$$

With

$$\tilde{S} = \left|\frac{\partial u}{\partial y}\right| + \frac{\vec{v}_t}{\kappa^2 d^2}f_{v_2} \qquad (2.9)$$

2.2.2. Shear Stress Transport Turbulence Model

Shear Stress Transport (SST) turbulence model was introduced by Menter in 1993. In the paper, two different turbulence models are presented.[17] First one is the baseline (BSL) model. The baseline model is a successive combination of k-ω and k-ε models. It uses k-ω model through the region close to the wall and switches to k-ε model for the outer part. The drawback of BSL model is similar to the standard k-ω model. The BSL still underpredicts the adverse pressure gradients under separation. Therefore, a modification to this model must be applied. Transport effects are taken into consideration for this modification. Accordingly, the second model, SST, is constructed. In this model as its name indicated eddy viscosity is defined by including the effect of transportation of principal shear stress. The turbulence model defines the eddy viscosity as follows in which $a_1 = 0.31$ the function $F_2 = \tanh(\text{arg}_2^2)$. In the function y denotes the margin from the wall.[15][18][17]

$$\varepsilon_m = \frac{a_1 k}{\max(a_1\omega, \Omega F_2)}$$

$$\text{arg}_2 = \max\left(\frac{2\sqrt{k}}{0.09\omega y}; \frac{500v}{y^2\omega}\right) \qquad (2.10)$$

12

The supersonic converging diverging nozzle has compressible flow inside of it Therefore, the transport equations for SST turbulence model can ben expressed as follows.

$$\frac{D\varrho k}{Dt} = \frac{\partial}{\partial x_k}\left[(\mu + \sigma_k \varrho \varepsilon_m)\frac{\partial k}{\partial x_k}\right] + R_{ik}\frac{\partial \bar{u}_i}{\partial x_k} - \beta^* \varrho \omega k \tag{2.11}$$

$$\frac{D\varrho\omega}{Dt} = \frac{\partial}{\partial x_k}\left[(\mu + \sigma_\omega \varrho \varepsilon_m)\frac{\partial \omega}{\partial x_k}\right] + \frac{\gamma}{\varepsilon_m}R_{ik}\frac{\partial \bar{u}_i}{\partial x_k}$$
$$- \beta \varrho \omega^2$$
$$+ 2(1-F_1)\varrho \sigma_{\omega_2}\frac{1}{\omega}\frac{\partial k}{\partial x_k}\frac{\partial \omega}{\partial x_k} \tag{2.12}$$

$$R_{ik} = \varrho \varepsilon_m\left(\frac{\partial \bar{u}_i}{\partial x_k} + \frac{\partial \bar{u}_k}{\partial x_i} - \frac{2}{3}\frac{\partial u_j}{\partial x_j}\delta_{ik}\right) - \frac{2}{3}\varrho k \delta_{ik} \tag{2.13}$$

As it can be seen the ε-equation converted to ω-equation by using cross-diffusion terms-. The F_1 term is an actually a way to compose the k- ω and k- ε turbulence models as explained. In the vicinity of boundary layer k- ω turbulence model is dominant whereas in the freestream k- ε model is dominant. Therefore, F_1 term can be expressed as follows with cross diffusion-term.

$$F_1 = \tanh(arg_1^4) \tag{2.14}$$

$$arg_1 = \min\left[max\left(\frac{\sqrt{k}}{0.09\omega y};\frac{500\nu}{y^2\omega}\right);\frac{4\varrho \sigma_{\omega_2}k}{CD_{k\omega}y^2}\right] \tag{2.15}$$

$$CD_{k\omega} = \max\left(2\varrho \sigma_{\omega_2}\frac{1}{\omega}\frac{\partial k}{\partial x_k}\frac{\partial \omega}{\partial x_k}, 10^{-20}\right) \tag{2.16}$$

In the turbulence model the fixed values are:

$$\beta^* = 0.09, \quad \kappa = 0.41 \tag{2.17}$$

The formula contains coefficient that are denoted by β, γ,σ_k and σ_ω. In the k- ω the tag $\phi = \{\sigma_k, \sigma_\omega, \beta, \gamma\}$ is called as ϕ_1 whereas in k- ε it is ϕ_2.

$$\phi = F_1\phi_1 + (1-F_1)\phi_2 \tag{2.18}$$

13

The coefficients are defined as follows for the inner model.

$$\sigma_{k_1} = 0.85, \quad \sigma_{\omega_1} = 0.5, \quad \beta_1 = 0.075$$

$$\gamma_1 = \frac{\beta_1}{\beta^*} - \frac{\sigma_{\omega_1} \kappa^2}{\sqrt{\beta^*}} = 0.553 \tag{2.19}$$

For the outer one the coefficients are also given.

$$\sigma_{k_2} = 1.0, \quad \sigma_{\omega_2} = 0.856, \quad \beta_2 = 0.0828$$

$$\gamma_2 = \frac{\beta_2}{\beta^*} - \frac{\sigma_{\omega_2} \kappa^2}{\sqrt{\beta^*}} = 0.440 \tag{2.20}$$

2.3. Numerical Discretization

In this part, the theoretical background of flow calculations is investigated. Firstly, Jameson Schmidt Turkel (JST) scheme is explained as a numerical solution method for the application of NSE. Secondly, computational grid generation is the subject of interest.

Convective flux terms can be calculated by several methods in SU^2.[5][19] In this study JST is chosen as the flux vector splitting scheme. In this method, artificial diffusion is used by calculating Laplacians in 2 different forms.[20][21]

For the unstructured grids the scheme can be expressed as:

$$\tilde{F}_{c_{ij}} = \tilde{F}(U_i, U_j) = \vec{F}^c \left(\frac{U_i + U_j}{2} \right) \cdot \vec{n}_{ij} - d_{ij} \tag{2.21}$$

There is also an addition to artificial diffusion.

$$d_{ij} = \left(\varepsilon_{ij}^{(2)} (U_j - U_i) - \varepsilon_{ij}^{(2)} (\nabla^2 U_j - \nabla_i^2) \right) \varphi_{ij} \lambda_{ij} \tag{2.22}$$

In the artificial diffusion term Laplacian terms are used for the neighboring nodes which can be defined as follows.

$$\nabla^2 U_i = \sum_{k \in \mathcal{N}} (U_k - U_i), \tag{2.23}$$

14

$$\lambda_{ij} = \left(\left| u_{ij} \cdot \vec{n}_{ij} \right| + c_{ij} \right) \Delta S$$

$$\lambda_i = \sum_{k \in \mathcal{N}(i)} \lambda_{ik}$$

$$\varphi_{ij} = 4 \frac{\varphi_i \varphi_j}{\varphi_i + \varphi_j}$$

$$\varphi_i = \left(\frac{\lambda_i}{4\lambda_{ij}} \right)^p$$

$$\varepsilon_{ij}^{(2)} = \kappa^{(2)} s_2 \left(\frac{\left| \sum_{k \in \mathcal{N}(i)} (p_k - p_i) \right|}{\sum_{k \in \mathcal{N}(i)} (p_k + p_i)} \right)$$

2.4. Computational Grid

In computational fluid dynamics most of the applications are modeled with NSE or other partial differential equations. These partial differential equations are impossible to solve directly. Therefore, they require a linearization and discretization process. The discretized partial difference equations are based on the options of modeling a computational domain which are Finite Volume Method (FVM), Finite Difference Method (FDM) or Finite Element Method (FEM).

As mentioned in this study FVM will be used as a modeling technique for partial difference equations. In order to make flow domain appropriate for finite volume method the domain must be decomposed into smaller domains which are called cells. These cells are the components of grid to be constructed through flow-field. In two dimensional applications, the domain is modeled with structured or unstructured grid. The difference between structured and unstructured grid yields on how the neighboring cells are defined.[22] In structured grid, the neighboring cells are numbered with simple arithmetic operations. On contrary, in unstructured grids all the cells are tabulated with their neighbors since their numbering is complex with respect to structured grids. Therefore, structured grids can easily be represented by matrices unlike unstructured grids.

For two dimensional applications a structured grid may be composed of triangles or quadrilaterals. The way that the structured grid is restricted and must be kept simple. However, unstructured grids can be constructed with many geometrical shapes and there are plenty of ways to build unstructured grid through a computational domain.

In this study, the computational domain is constructed with unstructured mesh generation. The chosen technique for mesh generation is Delaunay Triangulation.

2.5. Optimization Procedure

The optimization procedure used in the current study is as follows:

- ❖ Generation of grid for a baseline geometry to determine the flow field characteristics inside of a supersonic converging-diverging nozzle

- ❖ Obtaining computational fluid dynamics results of the nozzle for given boundary conditions

- ❖ Generating free form deformation boxes for the design optimization interests

- ❖ Evaluation of gradients for the flow field with adjoint flow solver

- ❖ Deforming the former geometry acccording to calculated gradients

- ❖ Obtaining the new objective function value with new geometry

The whole flow simulation and optimization procedure is processed on SU^2. Therefore, the processes can be summarized in the .
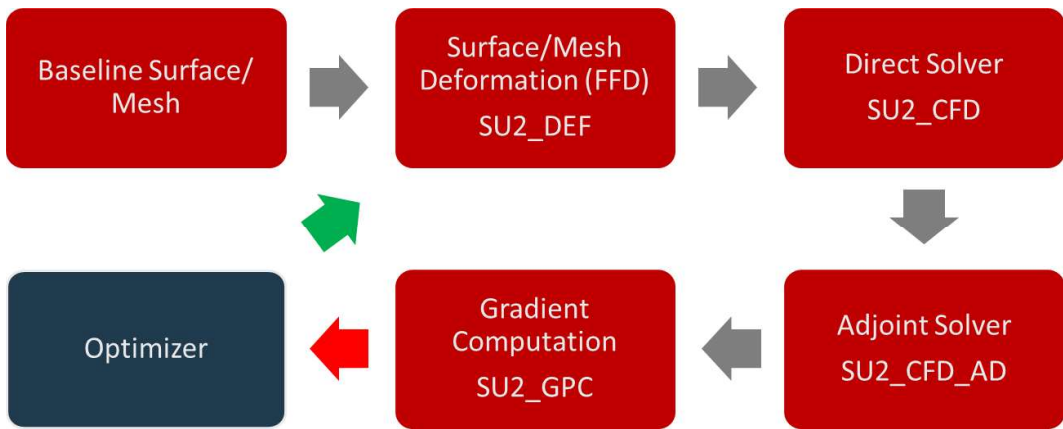
Figure 2.1. Optimization Process

2.6. Optimization Method

SU^2 optimization process mainly consists of surface deformation code which deforms the baseline geometry within the limitations of free form deformation (FFD) boxes, flow solvers which solves the Navier-Stokes/Euler equations for the problem to be investigated, adjoint solver which calculates sensitivities, gradient computation tool and the optimizer.

2.6.1. Shape Deformation

An optimization procedure starts with a baseline geometry. The baseline geometry is surrounded by a grid like structure which contains the control points to be deformed. Free Form Deformation (FFD) method enables the geometry to deform continuously from the required locations since it assumes the material of geometry as flexible as possible. As a result of this there can't be a surface discontinuity along the geometry. An illustration of FFD box concept is represented in the Figure 1.1.
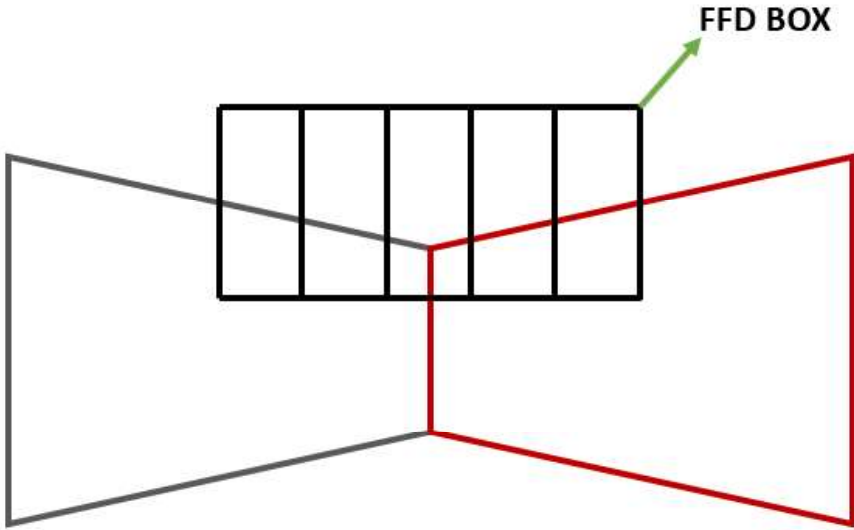
Figure 2.2. FFD Box Illustration

In SU^2 code Bezier curve functions are available for use in the FFD shape deformation option. The cartesian coordinates of X (i,j,k) are parametrized by using ξ, η, ς in degree of l, m, n.[23]

$$X(\xi, \eta, \varsigma) = \sum_{i=0}^{l}\sum_{j=0}^{m}\sum_{k=0}^{n} P_{i,j,k} B_i^l(\xi) B_j^m(\eta) B_k^n(\zeta) \qquad (2.24)$$

Bezier's control volume is demonstrated through polynomials called polynomials of Bernstein. According to the design area the control points of an FFD box is determined in harmony with the type of Bernstein polynomial to be used. These polynomials are denoted with B as in the equation following.[23]

$$\begin{cases} B_i^l(\xi) = \dfrac{l!}{i!\,(l-i)!}\,\xi^i(1-\xi)^{l-i} \\[2mm] B_j^m(\eta) = \dfrac{m!}{j!\,(m-j)!}\,\eta^i(1-n)^{m-j} \\[2mm] B_k^n(\zeta) = \dfrac{n!}{k!\,(n-k)!}\,\zeta^k(1-\zeta)^{n-k} \end{cases} \tag{2.25}$$

After design vectors, α, are assigned in order to insert mesh deformation; the new grid, X, goes into the evaluation of state variables U. Accordingly, the objective function J calculated for every iteration. [24]
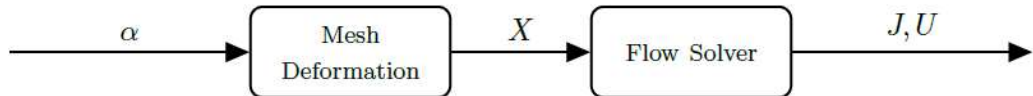
Figure 2.3. Aerodynamic Design Chain[24]

2.6.2. Adjoint-Based Optimization

Gradient calculation needs to be done in a way that is correct and effective. Search for an optimized geometry needs this feature since it is an expensive procedure. SU^2 basically overcomes the gradient evaluation as expressed in the equation. [23]

$$\begin{bmatrix} \dfrac{\partial f}{\partial x_1} \\[2mm] \dfrac{\partial f}{\partial x_2} \\[1mm] \vdots \\[1mm] \dfrac{\partial f}{\partial x_n} \end{bmatrix} = \begin{bmatrix} \dfrac{\partial s_1}{\partial x_1} & \cdots & \dfrac{\partial s_m}{\partial x_1} \\[2mm] \vdots & \ddots & \vdots \\[2mm] \dfrac{\partial s_1}{\partial x_n} & \cdots & \dfrac{\partial s_m}{\partial x_n} \end{bmatrix} \begin{bmatrix} \dfrac{\partial f}{\partial s_1} \\[2mm] \dfrac{\partial f}{\partial s_2} \\[1mm] \vdots \\[1mm] \dfrac{\partial f}{\partial s_m} \end{bmatrix} \tag{2.26}$$

The terms of the equation can be explained as:

$$Gradients = Geometric\ Sensitivities\ x\ Surface\ Sensitivities \tag{2.27}$$

19

In the equation x is the design variables whereas f represents the objective function. Also, s is the surface normal of the given control points.

Adjoint method is applied to aerodynamic applications by Jameson in 1980's. The flow equations are partial differential equations they require high number of iterations for solution. In order to calculate sensitivities, adjoint method introduces variables and creates its own equations. Therefore, adjoint method simplifies the calculation of sensitivities. Adjoint method is divided into two as continuous and discrete method. These two methods are illustrated in the following Figure 2.4.[19]
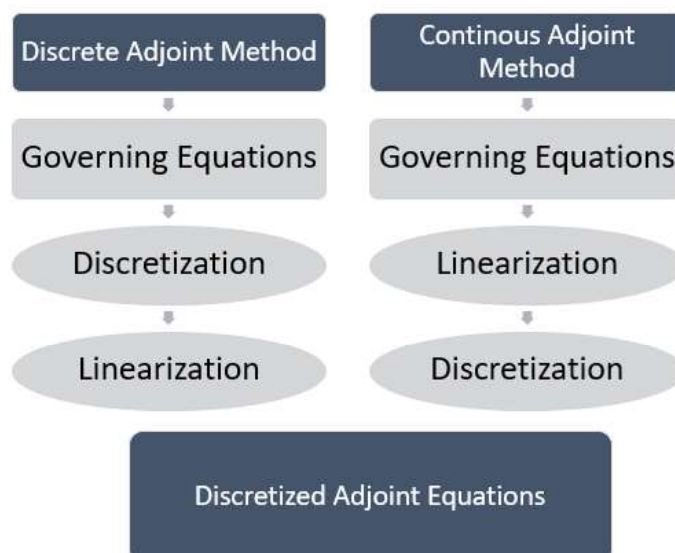
Figure 2.4. Discrete and Continuous Adjoint Methods

As seen from the schematic discrete and continuous adjoint method differs from each other in terms of order in discretization and linearization. In the discrete approach, gradients are supplied precisely because it requires simply a transpose operation to governing equations with less work with respect to continuous approach. On contrary, continuous approach gives estimation of gradients.[25]

In aerospace applications like nozzle optimization cases, symmetrical properties of a design must be satisfied. However, in continuous adjoint based optimization processes; complication during derivation of adjoint equations may result in asymmetrical properties. Moreover, this problem may cause difficulties in convergence.[26] Unlike discrete approach, continuous adjoint method leads physically well-defined sets of equations and offers more solution methods. As an example, shocks occurring the flow field can be well understood by adjoint flow solutions due to purely characterized boundary conditions.[27] Also, storage requirement of continuous approach is less compared to discrete one.[28]

In the discrete approach, on contrary to continuous approach, convergence is guaranteed due to the fact that whole equations are based on evaluations of exact gradients. This also allows an algorithm based on discrete approached to be programmed easily.[27] The matrix constructed with discrete adjoint equations shares same eigenvalues with the original PDE itself. Therefore, iterations are robust compared to iterations of continuous approach. Also, the systematic representation of discrete adjoint approach enables equations set for AD.

As a final step of continuous or discontinuous approach, gradient of a function is calculated by using AD in SU^2. In AD, by using all the design variables; whole code is algorithmically differentiated. Since there is no explicit definition of derivative term in this differentiation technique, there is no truncation error like in finite difference technique. Therefore, this makes AD superior to finite difference in terms of truncation error. Also, with this implementation to SU^2 makes it possible to obtain discrete adjoints available right after an iteration without any additional attempt. [24][29]

In SU^2 after obtaining flow solution with the governing equations, such as RANS, the adjoint variables are evaluated with the following notation. In the equation, it is must be noted that flow variables defined by U, viscous F^v and convective F^c fluxes are defined. Equation also contains residual R and a source term Q.[23]

$$\frac{\partial U}{\partial t} + \nabla \cdot F^c - \nabla \cdot F^v - Q = R \qquad (2.28)$$

During this study, RANS equation is solved by a FVM which is JST as mentioned by using SST and SA turbulence models. After flow solution, adjoints of the system are evaluated.[23] In this adjoint equation, $i,j = 1,2,3$, μ_{tot} represents the viscosity and Ψ denotes adjoint variables.

$$\frac{\partial \Psi}{\partial t} - \nabla \Psi \cdot \left[\left(\frac{\partial F^c}{\partial U} \right)_i - \mu_{tot} \left(\frac{\partial F^v}{\partial U} \right)_i \right] - \nabla \cdot \left[\nabla \Psi \cdot \mu_{tot} \frac{\partial}{\partial x_j} \left(\frac{\partial F^v}{\partial U} \right)_i \right]$$
$$- \frac{\partial Q}{\partial U} = 0 \qquad (2.29)$$

2.6.2.1. Discrete Adjoint Approach

In SU^2 the implementation of discrete adjoint approach accomplishes governing equations to give Lagrangians in a relationship with residues $\mathcal{R}_p$ defined in following equation. [19]

$$\mathcal{L} = \mathcal{J}_D + \sum_{p=1}^{N} \psi_p^T \mathcal{R}_p \qquad (2.30)$$

In the equation defining Lagrangians ψ represent the Lagrange multipliers and disturbance in Lagrangian given as follows.

$$\Delta \mathcal{L} = \Delta \mathcal{J}_D + \sum_{P=1}^{N} \psi_p^T \Delta \mathcal{R}_p \qquad (2.31)$$

There is also a discrete Jacobian designated with elimination of disturbance. Therefore, a perturbation to the objective function $\Delta \mathcal{J}_D$ is obtained.

$$\sum_{q}^{N} \left(\frac{\mathcal{D} R_q}{\mathcal{D} U_p} \right)^T \psi_q = - \left(\frac{\mathcal{D} \mathcal{J}_D}{\mathcal{D} U_p} \right)^T \qquad (2.32)$$

$$\Delta \mathcal{J}_D = \sum_p^N \psi_p^T \left(\frac{\mathcal{D}\mathcal{R}_p}{\mathcal{D}\alpha} \right) \Delta\alpha + \frac{\mathcal{D}\mathcal{J}_D}{\mathcal{D}\alpha} \Delta\alpha$$

2.6.2.2. Continuous Adjoint Approach

Implementations to SU^2 requires the solution of analytical governing equations to give $\{\mathcal{N}\} = 0$ with designated Lagrange multiplier ϕ.[19]

$$\mathcal{L} = \mathcal{J}_C - \int_\Omega \phi^T \mathcal{N} d\Omega \qquad\qquad 2.33$$

Accordingly, in the continuous approach perturbation to the Lagrangians $\delta\mathcal{L}$ becomes;

$$\delta\mathcal{L} = (\mathcal{J}_C' - \mathcal{J}_C) - \left(\int_{\Omega'} \phi^T \mathcal{N}' d\Omega - \int_\Omega \phi^T \mathcal{N} d\Omega \right) \qquad\qquad 2.34$$

CHAPTER 3

RESULTS & DISCUSSION

In this part of the thesis, firstly a verification is presented in Section 3.1. After the SU^2 is verified, shape optimization results are given in Section 3.2. These results are separated into two subgroups, according to the location of the FFD box.

3.1. Verification

A two-dimensional nozzle experiment in the literature is compared with the results of various computational fluid dynamics solutions of SU^2. In the study, firstly, the verification case is described with its geometrical properties, boundary conditions and experimental information. Secondly, a grid independence study is conducted. The grid convergence study basically consists of four different cases with four different grids. These grids differ from each other by resolution. Finally, the effect of turbulence model on the solution is investigated by using SST and SA models.
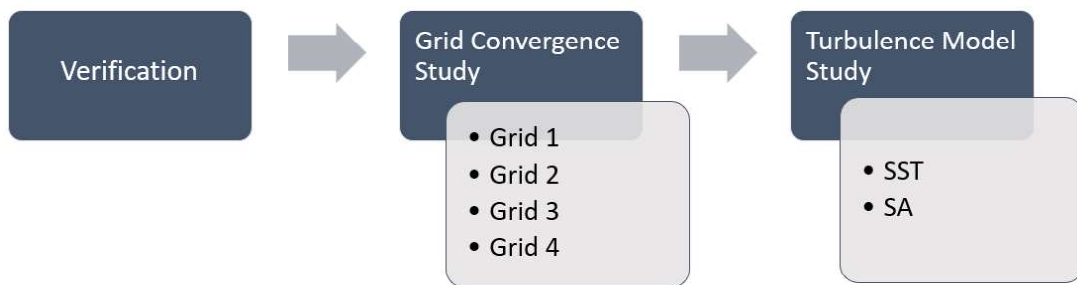
Figure 3.1 Verification Process Schematic

After all the cases considered, optimization procedure starts with the chosen grid and with the two turbulence models.

3.1.1. Verification Case Description

In order to prove that the results of SU^2 is valid an experimental study must be used to compare the solutions of it. To verify the solution, experimental work done by Kostic et Al is used. The test section used in this work is given in Figure 3.2.[30]
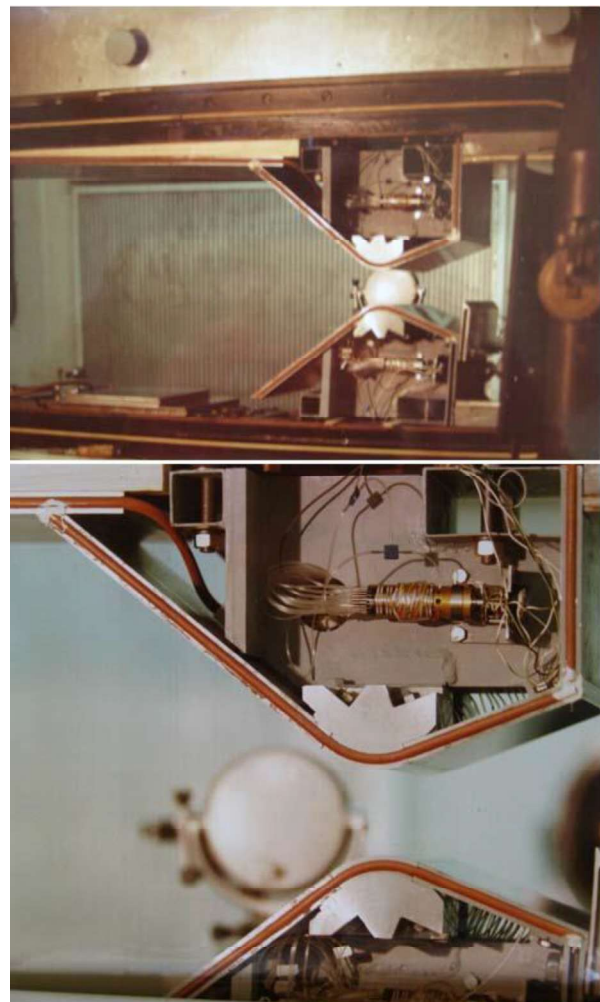
Figure 3.2. Test Section [30]
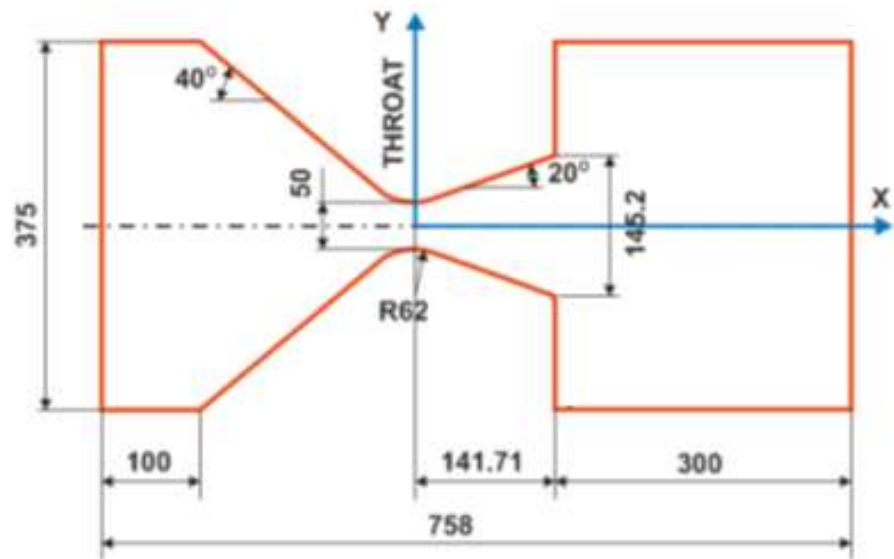
Figure 3.3. Geometry Specifications [30]
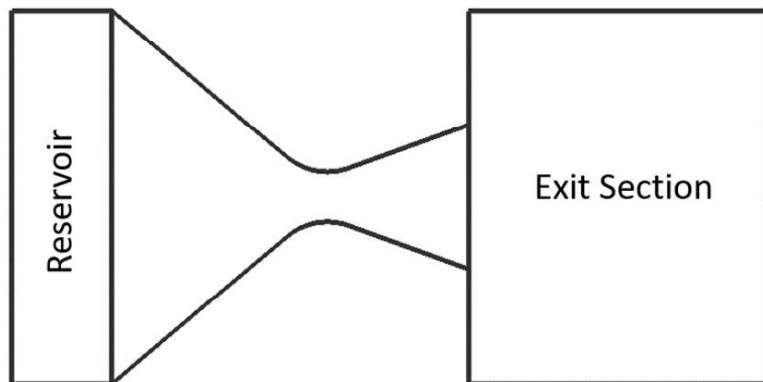
Figure 3.4. Reservoir and Exit Section

The experimental study is processed by using wind tunnel of Military Technical Institute VTI Zarkovo. A rectangular cross-sectional two-dimensional nozzle that have an exit Mach number around 2.6 is the subject of this work. The control volume consists of reservoir, nozzle and the 300 mm long outlet region. The geometry specifications of the nozzle are given in Figure 3.3.[30] The reservoir and exit section of the test setup are given in . [30]

The reservoir pressure and temperature, flow Mach number entering the nozzle, atmospheric pressure at the exit of the nozzle are also specified in the paper where experimental work is done. Therefore, these boundary conditions are tabulated in following table.

Table 1. Boundary Conditions [30]

Region	M	T [K]	P[Pa]
Reservoir	0.086	286.75	101831.3
Exit	-	-	500

In the exit section 500 Pa pressure is achieved by using vacuum tanks. The reservoir has the nominal Mach number of 0.086, static pressure 101831.3 Pa and temperature 286.75 K. The working fluid of the experiment is air.
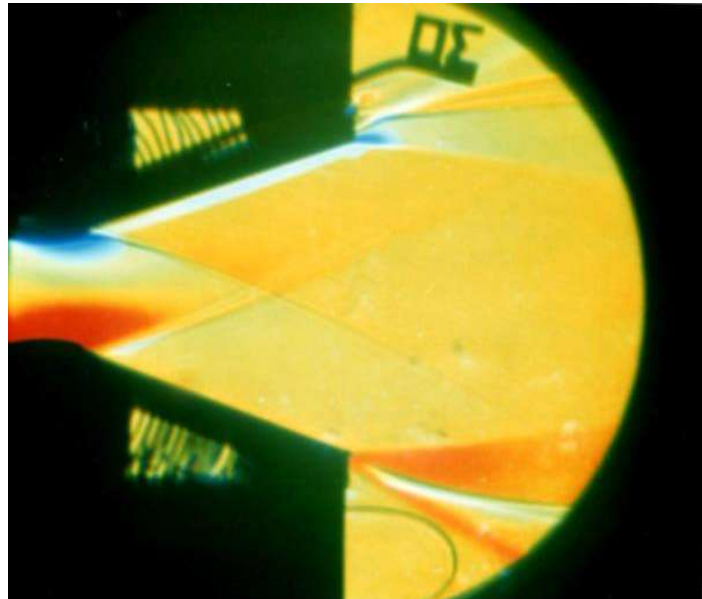
Figure 3.5. Schlieren Photo of the Flow [30]

During the experiments flow field of the test section is observed by color Schlieren photography. The photographs obtained by this technique have inverted colors of the flow-field. Also, static pressure distributions from upper and lower divergent walls

are measured. A Schlieren photo of the flow through the nozzle domain is given in the paper (Figure 3.5).
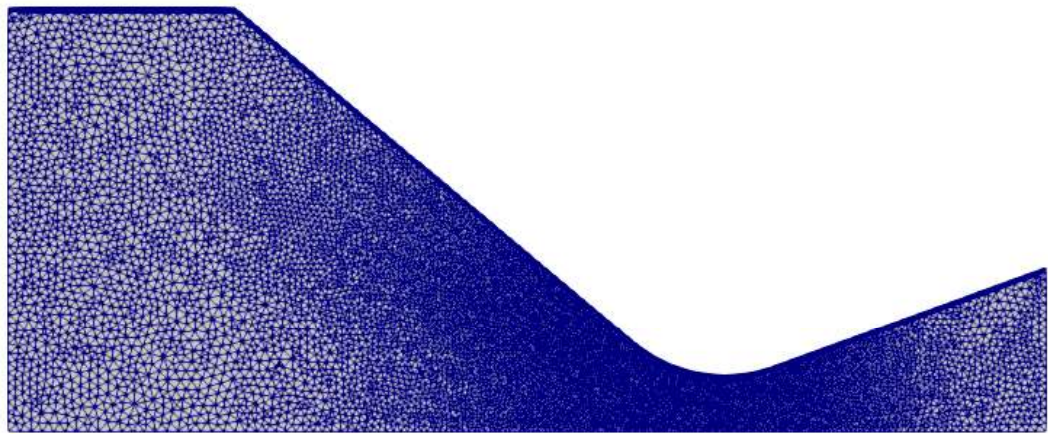
3.1.2. Grid Independence Study

In a computational fluid dynamics application flow domain is divided into large number of small cells. With respect to the complexity of the investigated geometry domain can be composed of structured or unstructured cells. These cell groups that represent the flow domain are called grid or mesh. For a two-dimensional flow domain cells may be in quadrilateral or triangle form. The quality of generated grid is important for obtaining a well-converged solution in CFD applications. Therefore, a grid study must be processed to have a reliable solution. Wall-bounded flow domains have to consist of qualified grids in order to model the computational domain properly. Especially in flow through supersonic convergent-divergent nozzles throat section must be modelled with fine grids. The reason behind this, throat is the transition region where flow changes its regime from subsonic to supersonic. In addition to flow solutions, an optimization process is performed onto grid to be chosen from this study. Optimization process requires deformation of the baseline geometry and the grid. Accordingly, in order not to have poorly established grid topology all the grid cases consist of large number of small cells. The reason behind this is to solve the flow domain with high accuracy by using smaller cells.
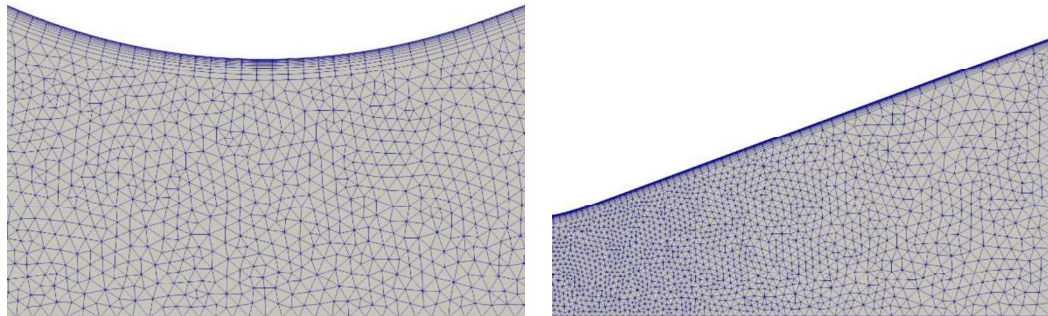
Table 2. Grid Study

Grid Name	*Triangles*	*Quadrilaterals*	*Total Number of Cells*
Grid 1	17,363	2,080	19,443
Grid 2	76,543	12,870	89,413
Grid 3	140,779	18,570	159,349
Grid 4	277,554	24,450	302,004

To show the differences between all four grids, their images are represented. The whole computational domains, closer screen shots to the throat and diverging section are displayed for better comparison.
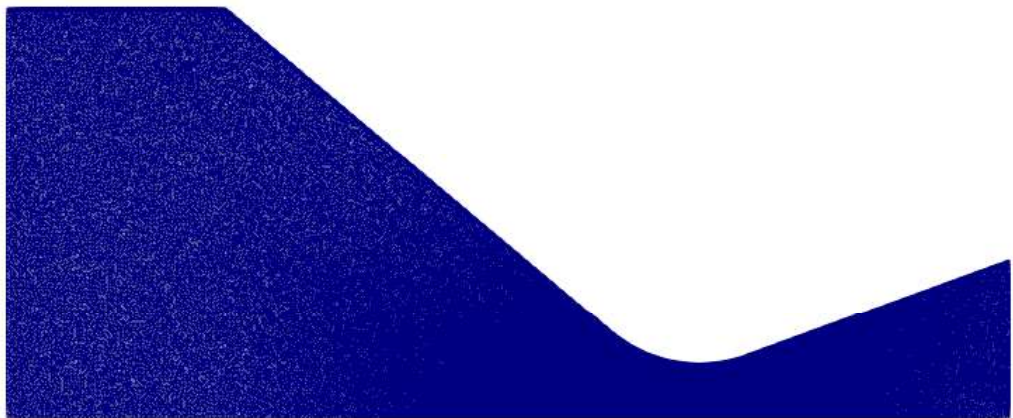
a
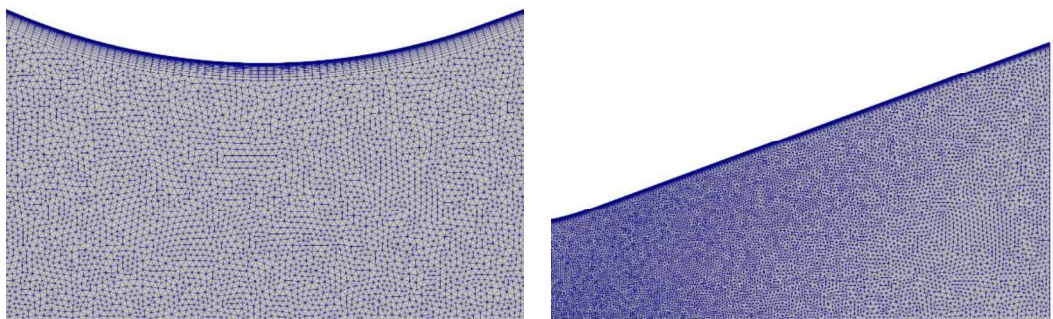
b   c

Figure 3.6. a) Computational Domain of Grid 1 with 17,363Triangles, 2,080 Quadrilaterals and 19,443Total Number of b) Cells Computational Grid of the Throat Section of Grid 1 c) Computational Grid of the Exit section of Grid 1

a
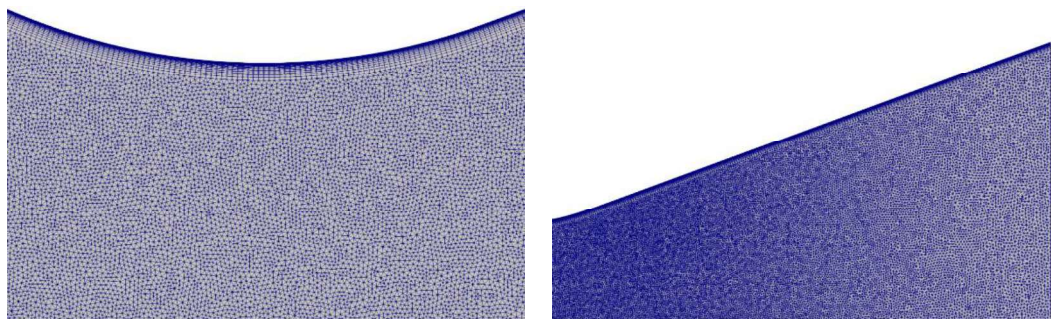
b   c

Figure 3.7. a) Computational Domain of Grid 2 with 76,543 Triangles, 12,870 Quadrilaterals and 89,413 Total Number of b) Cells Computational Grid of the Throat Section of Grid 2 c) Computational Grid of the Exit section of Grid 2
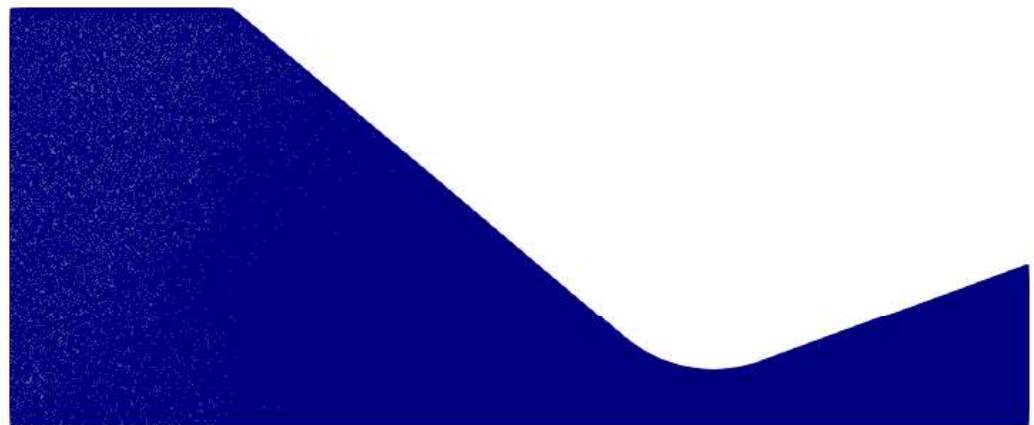
a
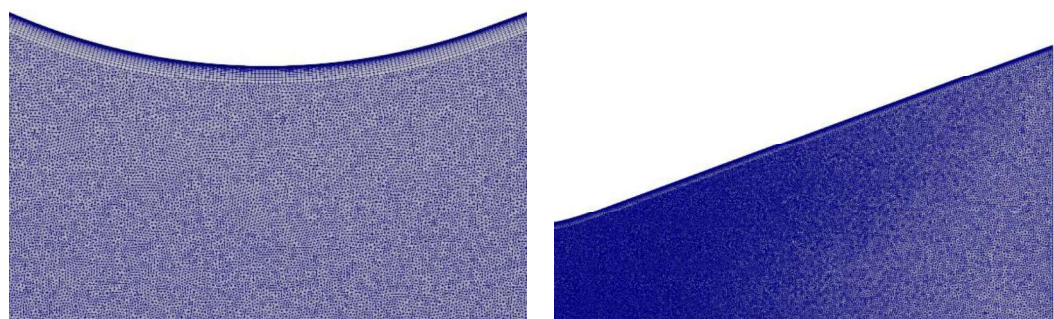
b   c

Figure 3.8. a) Computational Domain of Grid 3 with 140,779 Triangles, 24,450
Quadrilaterals and 159,349 Total Number of Cells b) Computational Grid of the Throat
Section of Grid 3 c) Computational Grid of the Exit section of Grid 3

a

b   c

Figure 3.9. a) Computational Domain of Grid 4 with 277,554 Triangles, 18,570
Quadrilaterals and 302,004 Total Number of Cells b) Computational Grid of the Throat
Section of Grid 4 c) 4 Computational Grid of the Exit section of Grid 4

To begin with 4 different grids are studied. Grid 1 is the one with coarser cells and Grid 4 has the highest number of cells. As it can be seen from the grids, they all consist of unstructured cells. After the validation, the free form deformation boxes will be constructed on these computational domains. Therefore, cells of the grids should not be skew after the deformation. The deformed grids must resolve the regions where deformation occurs. Accordingly, one must consider the skewness criteria after the deformation before choosing the appropriate grid. The most important part of a supersonic converging diverging nozzle is its throat section. Flow switches its regime from subsonic to supersonic. For this reason for all the cases smaller cells are used to model throat region.

For the grid convergence study, CFD solutions are obtained by using RANS equations with SST turbulence model. The FVM numerical discretization scheme is chosen as JST as mentioned. There is no multi-grid level is used for the solution. Fluid, air, is modeled as ideal gas with viscosity by Sutherland Law. Steady state analyzes are carried out until residuals converge to the same value for all the grids. In the experiment, upper and lower wall pressure distributions of divergent section are available. Therefore, for all the 4 grids upper and lower divergent wall pressure distributions are compared to each other. Moreover, in the reference there is CFD solution. This solution is obtained using ANSYS Fluent 14. In this CFD analysis, SST turbulence model, multi-grid solution method with 4 levels and density-based solver are used.[30]
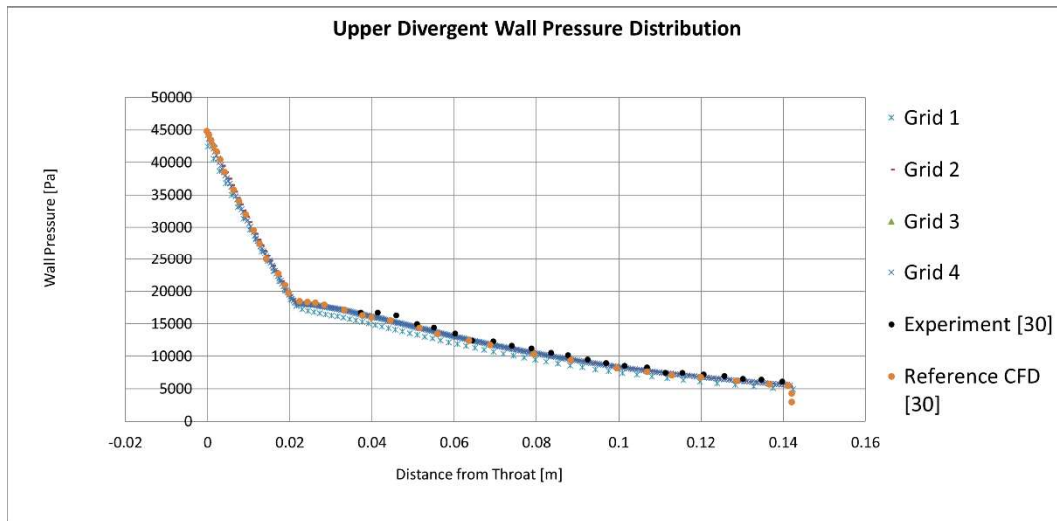
Figure 3.10. Upper Divergent Wall Pressure Distribution
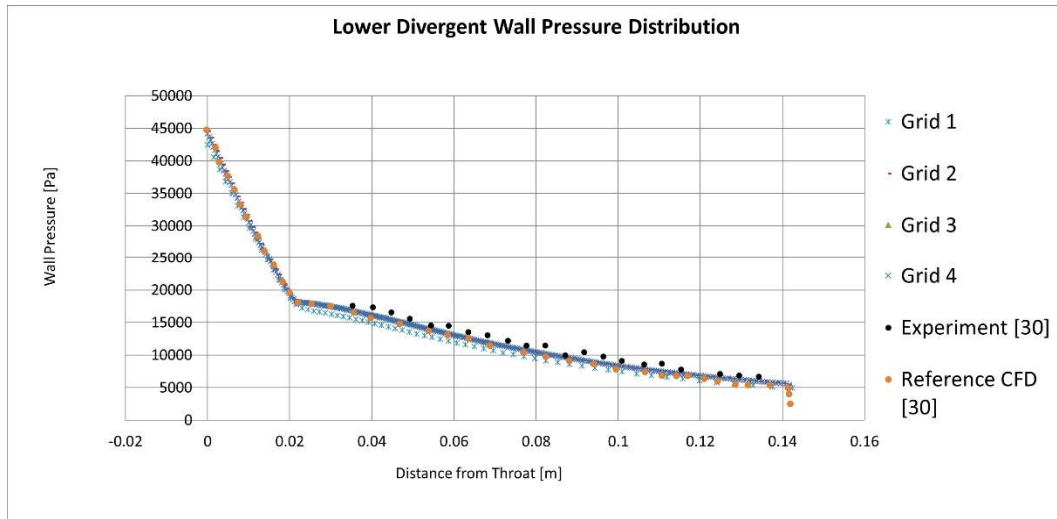
Figure 3.11. Lower Divergent Wall Pressure Distribution

The static pressure distributions of upper and lower divergent wall of the computational fluid dynamics solutions from all four grids are close to each other. As expected, static pressure along the wall decreases with expanding flow. They have the same behavior with the experimental and CFD result of the reference. However, Grid 1, gives slightly worse result than the other grids. This is due to the fact that Grid 1 has higher first layer thickness for the boundary layer calculations.
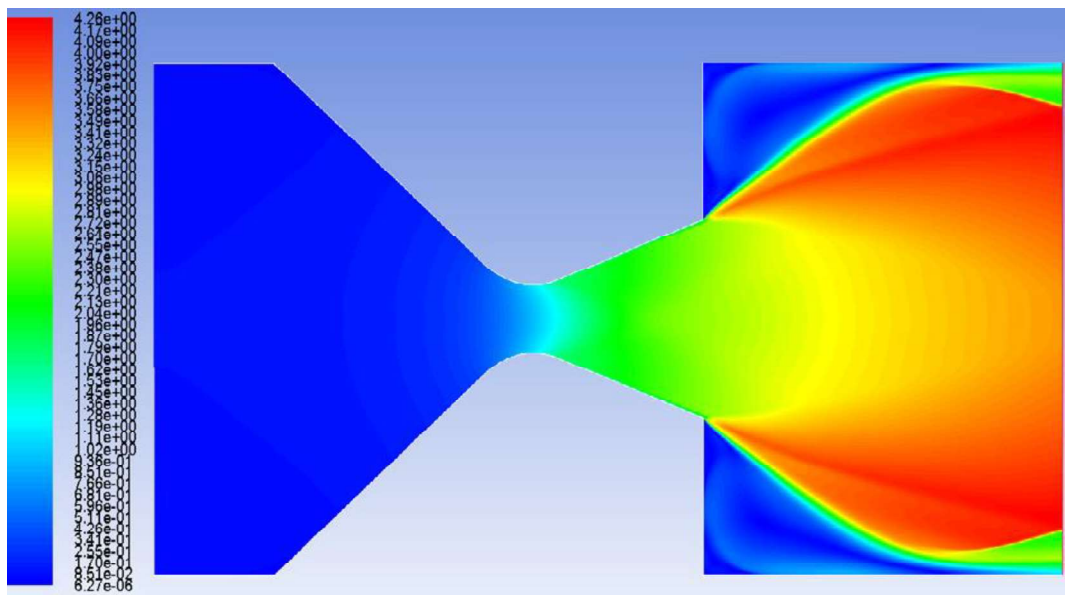
On contrary, other three grids have almost same results with respect to each other. Therefore, Grid 2 is chosen as the grid that is taken into action. Owing to its lower number of cells, it is considered that Grid 2 will take less time with respect to other two grids. Since every optimization process contains large number of flow simulations an optimum grid must be determined carefully to obtain required design.

In the reference, as mentioned there is also a computational fluid dynamics solution available. This solution of the reference work is obtained using ANSYS Fluent 14. In this CFD analysis, SST turbulence model, multi-grid solution method with 4 levels and density-based solver are used.

In the SU^2 solution; configuration file constructed with SST turbulence model. JST numerical scheme is used as the convective numerical method and no multi-grid is used.

To compare the result of SU^2 with Grid 2, Mach number contours of the both works are represented in Figure 3.12. To see the similarity legend of the SU^2 solution has been set to the solution of reference. Therefore, as it can be seen same trend during the expansion along supersonic converging diverging nozzle is achieved. Reaching the Mach number equals to 1 is achieved for SU^2 solution like the reference CFD result.

In addition, from the figure, it must be noted that experimental nozzle is under expanded. This can be understood by looking the behavior of working fluid right after the nozzle exit. The jet tends to expand in order to reach the ambient pressure where the nozzle spreads out. Therefore, this means nozzle configuration is insufficient to expand the fluid in order to reach ambient pressure.

a

b

Figure 3.12. Computational Fluid Dynamics Result a) Reference [30] b) SU^2

3.1.3. Turbulence Model Study

After selection of the grid to be used in the study, turbulence model must be assigned in order to move on. For this reason, SST and SA turbulence models are subjected to CFD analysis on the verification case. The comparison between the two turbulence models is represented on the basis of wall pressure distribution along the upper and lower divergent walls.

a

b
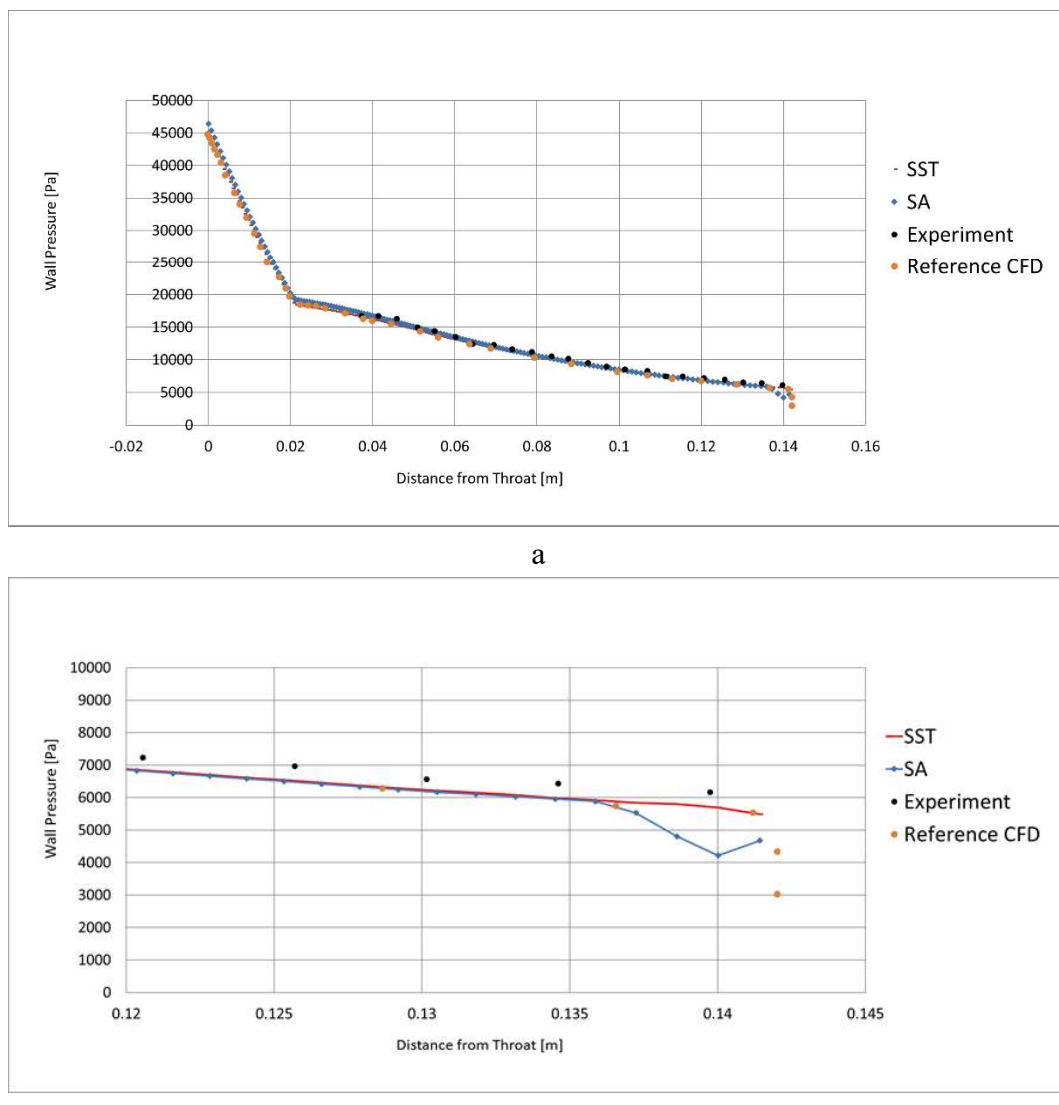
Figure 3.13. a) Upper Divergent Wall Pressure Distribution b) Upper Divergent Wall Pressure Distribution Near Exit Section

a

b
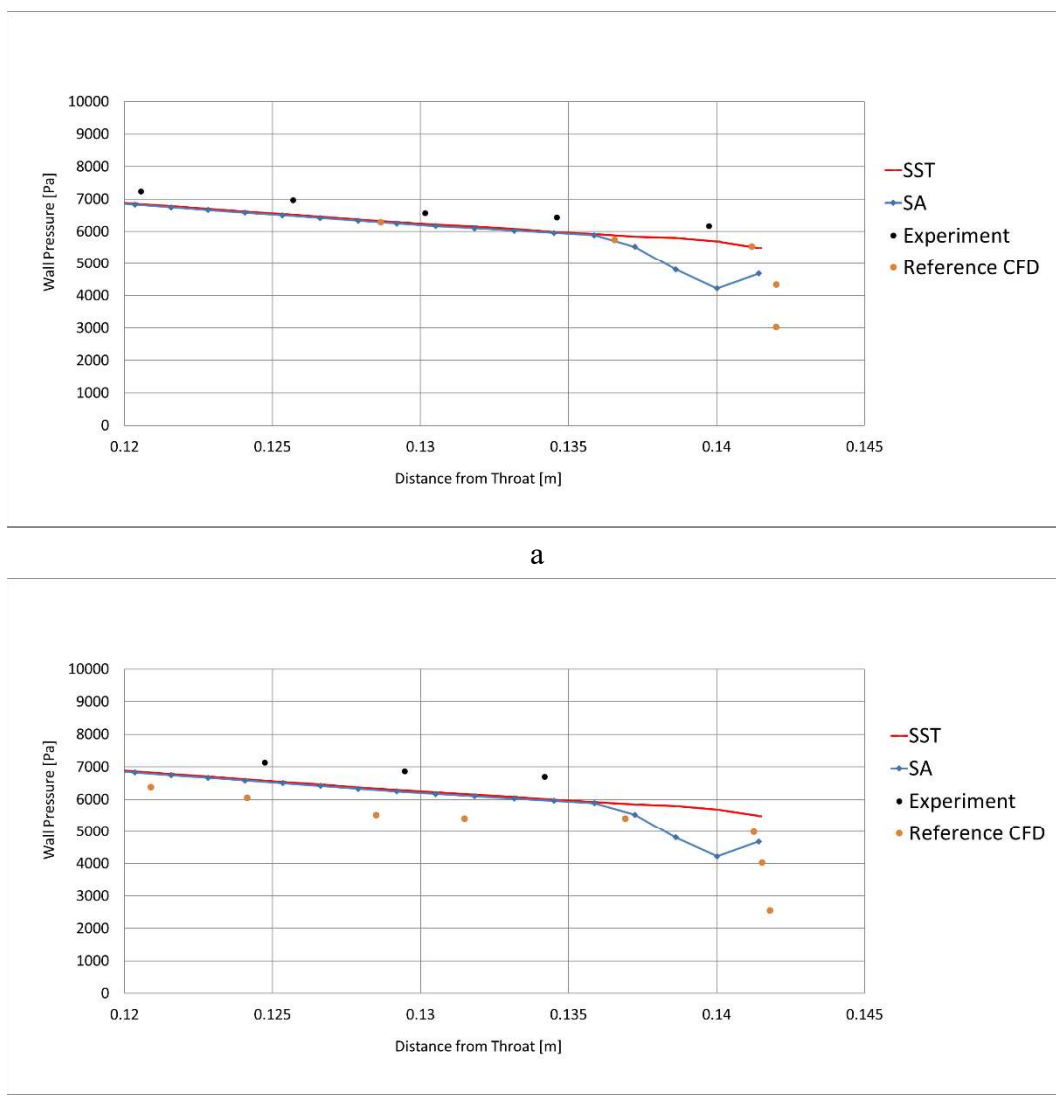
Figure 3.14. a) Lower Divergent Wall Pressure Distribution b) Lower Divergent Wall Pressure Distribution Near Exit Section

As it can be seen from wall pressure distributions, SST and SA models give similar results to each other. For the SA model, pressure drops down through the exit with an unphysical way (Figure 3.13 b, Figure 3.14 b). It differs from the reference CFD result and the SST turbulence model solution. The Mach number contours of SST turbulence model and SA turbulence model solutions are also represented to show that for the whole computational domain there is no glaring difference between them ,Figure 3.15. SST turbulence model follows the trend of experimental and CFD

result of the reference more. Therefore, after all the study outputs are considered, both SST turbulence model is decided to be used in the optimization procedure.

a

b
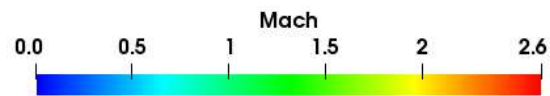
Figure 3.15. a) SST Turbulence Model Mach Number Result b) SA Turbulence Model Mach Number Result

3.2. Shape Optimization

In the shape optimization part; firstly, only the throat profile of the baseline geometry is encapsulated for geometry parametrization. After an optimization procedure based on Mach number maximization at the exit surface, it is seen that deforming only throat profile results in surface discontinuity in nozzle profile along the diverging section. This discontinuity causes a shock generated through the supersonic flow. Therefore, deformation of only throat profile considered as a poor way to optimize throat. Accordingly, geometry parametrization spreads out through diverging section until the nozzle exit. For the following studies, surface Mach number maximization, surface mass flow rate maximization, multi objective design study of those two parameters and multi objective design study with total pressure constraint are processed respectively (Figure 3.16).
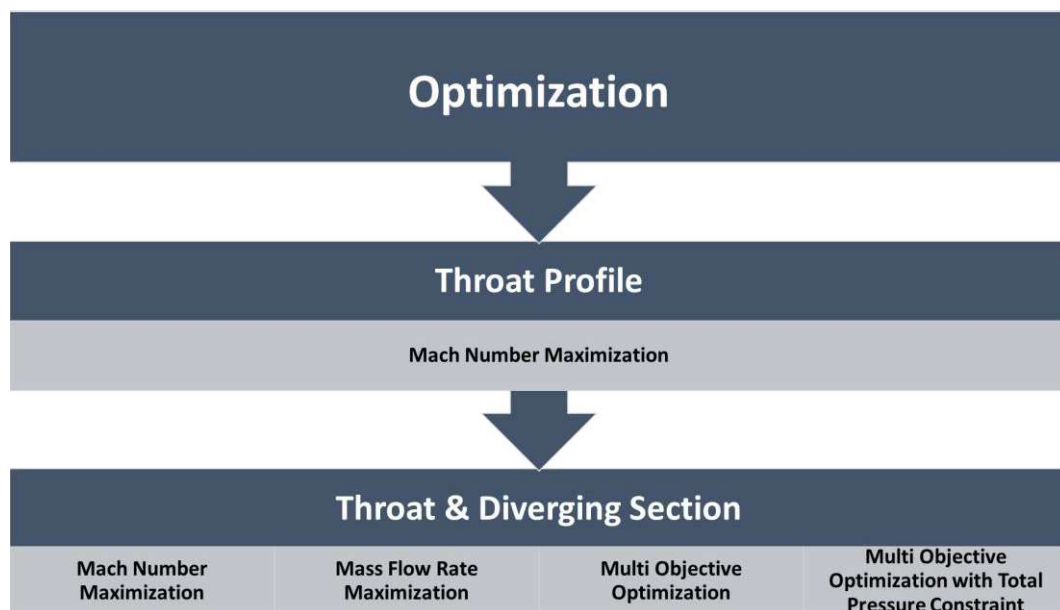
Figure 3.16. Optimization Studies

During these optimization studies discrete adjoint method is used. The CFD analyzes are carried out by using RANS equations with SST turbulence model. For the inlet boundary condition total pressure and total temperature is used. For the outlet boundary condition supersonic outlet is used.

41

3.2.1. Shape Optimization of Throat Profile

Throat is the most important part of a supersonic converging diverging nozzle concept. It drives the mass flow rate of the nozzle with having sonic Mach number through itself. Therefore, changing properties of throat section will be the most effective way to tune flow parameters.
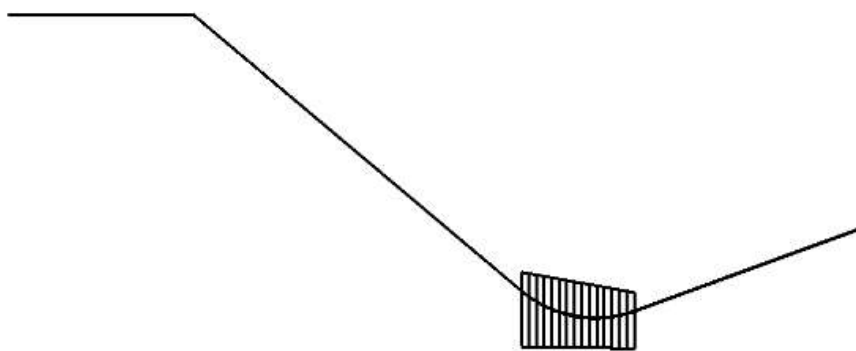
Figure 3.17. FFD Box Encapsulating Throat Section

In order to change the throat profile, FFD box is created so that it encapsulates whole throat profile. FFD box contains 15 design variables along its nodes crossing with the nozzle walls. After FFD box is created, the flow solution is subjected to a Mach number maximization process.

3.2.1.1. Mach Number Maximization

In this section, exit Mach number of the baseline nozzle is optimized. To do this only throat section of the geometry is deformed. Accordingly, only the throat and close neighboring region is surrounded by FFD boxes. The objective is to play with throat area and having an increase in Mach number at the exit section. The profile

comparison of baseline and final design is given in Figure 3.18. The average exit Mach number results of baseline and the final design are given in Table 3.

a   b

c   d
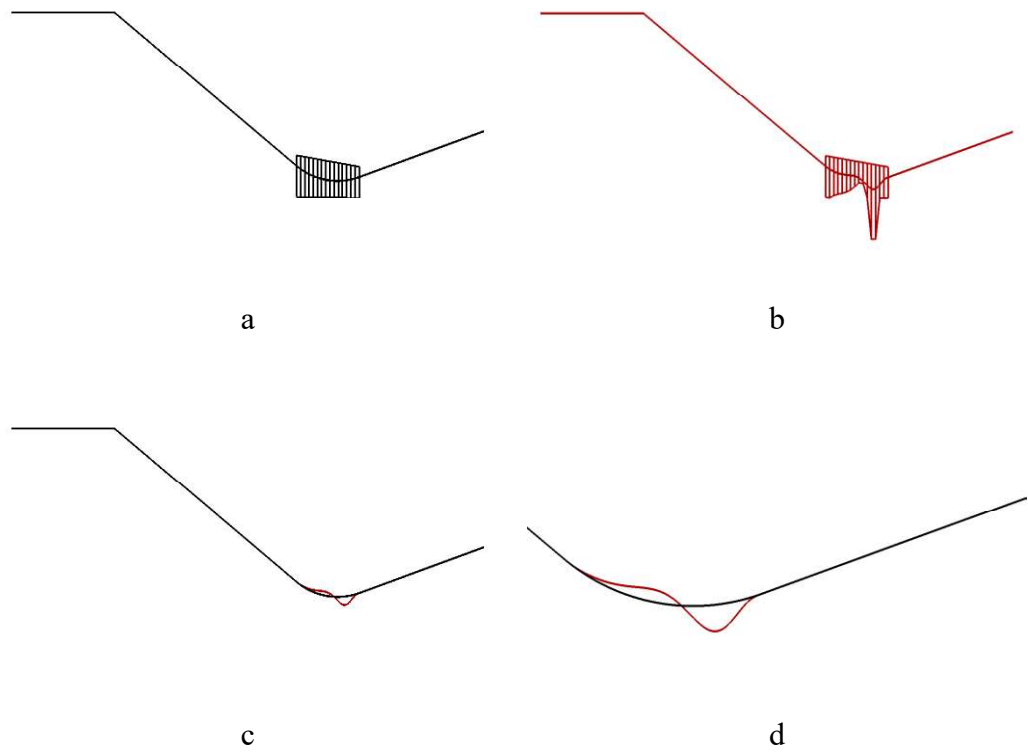
Figure 3.18. a) Baseline Geometry and Undeformed FFD Box b) Final Geometry and Deformed FFD Box c) Baseline and Final Geometry d) Baseline and Final Geometry Throat Profile

Table 3. Exit Mach Number and Throat Radius of Baseline Geometry and Final Design

Design	Exit Mach Number
Baseline Geometry	2.56
Final Design	2.90

FFD box consists of 15 control points and it only has one degree of freedom which is in y direction. Consequently, idea here is changing the throat area smoothly and increase Mach number at the exit section of supersonic converging diverging nozzle. After iterations, baseline geometry is deformed according to sensitivities that are calculated after flow solution. As it can be seen from the comparison deformed geometry has lower throat area with respect to the baseline geometry. This is

because optimizer tries to reach sonic condition at throat with minimum area. Since area ratio between throat and the exit section is the main parameter that drives exit Mach number it makes sense to decrease throat area. Therefore, in order to compare the difference of change in throat profile, Mach number distributions for the baseline and the final designs are represented in Figure 3.19.
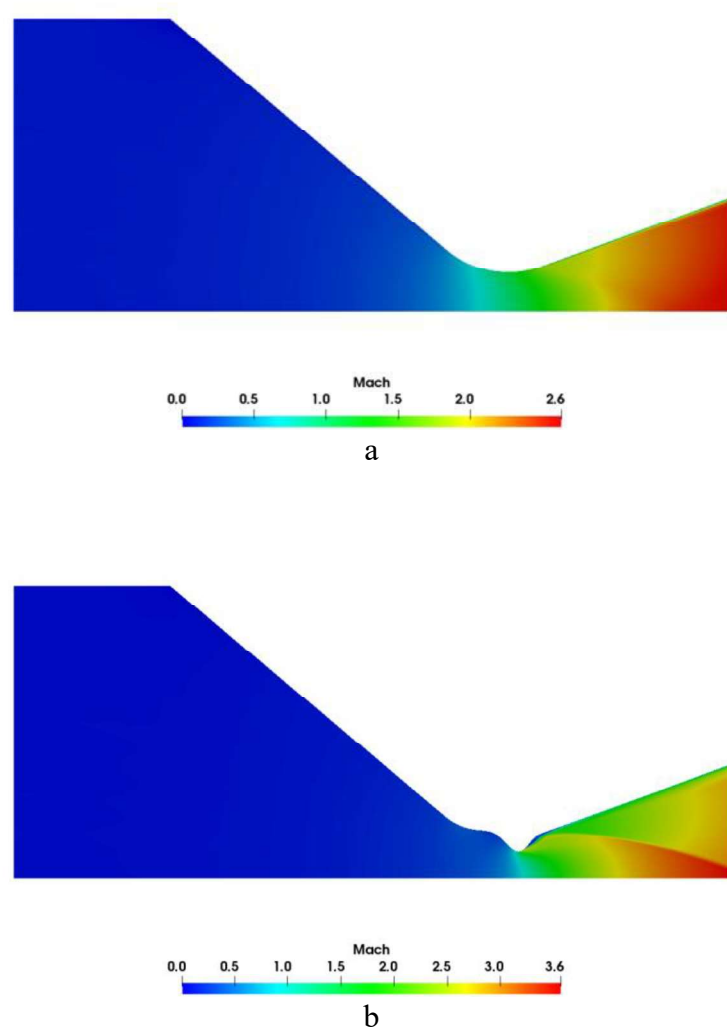
Figure 3.19. Mach Number Distribution of a) Baseline Design b) Final Design

As it can be seen from the Mach number contours, final design reaches higher maximum Mach number than the baseline design. However, there is a strong discontinuity in the flow field. This discontinuity appearing in the Mach number contour is caused by the optimizer trying to decrease throat. The decrease in throat area is smooth but the change throat profile cannot be followed by the remaining part of diverging section. Therefore, flow is forced to turn into itself and a discontinuity appears through the flow field.
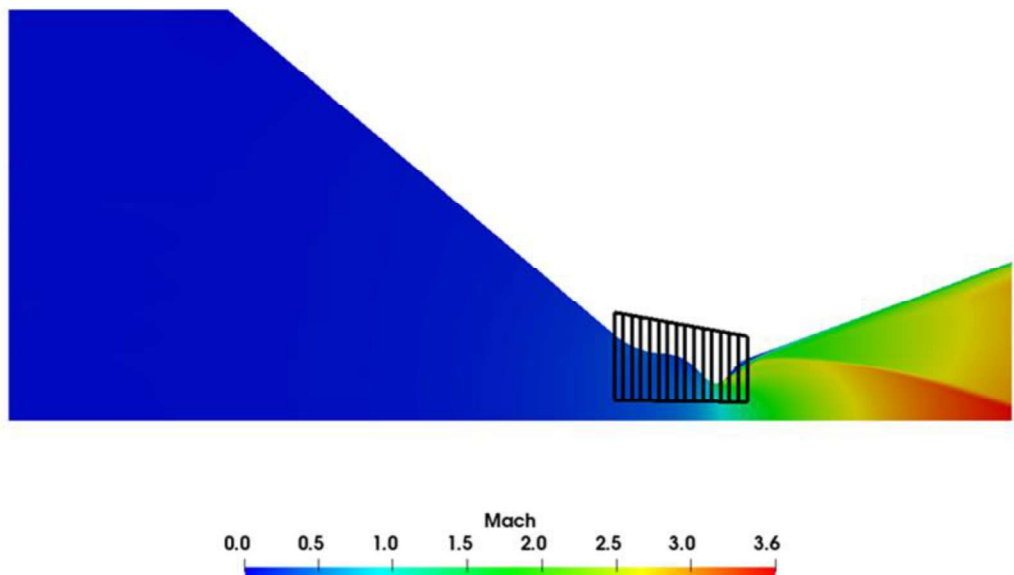
Figure 3.20. Mach Number Distribution of Final Design and FFD Box

As the FFD box covers only the throat section, changes in the geometry of the throat are independent of the divergent section. This may generate a discontinuous geometry that has an inflection point at the interface between the throat and the divergent section, causing an oblique shockwave as seen in Figure 3.20. In order to examine the difference, Mach number profiles at the exit are plotted in Figure 3.21. In this figure, y=0 m axis represents the symmetry plane, and wall is located at y=0.073 m. Although final design has higher Mach number at the exit than baseline

design, the uniformity of baseline is better than optimized geometry. The main reason of this difference is the discontinuity in final design.
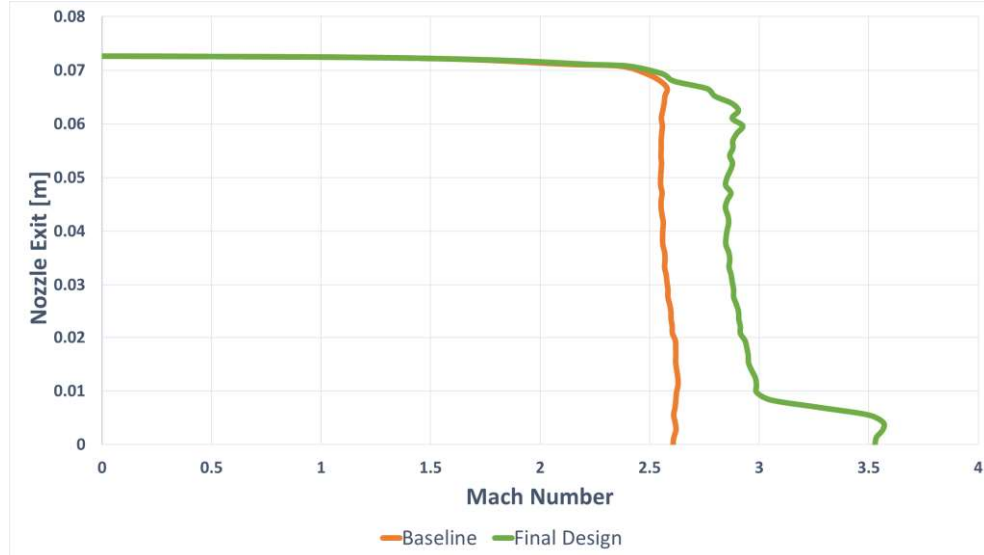
Figure 3.21. Mach Number Variation at the Exit

In addition to the Mach number profiles at the exit section, the distribution of axial component of momentum at the exit section is plotted in Figure 3.22.
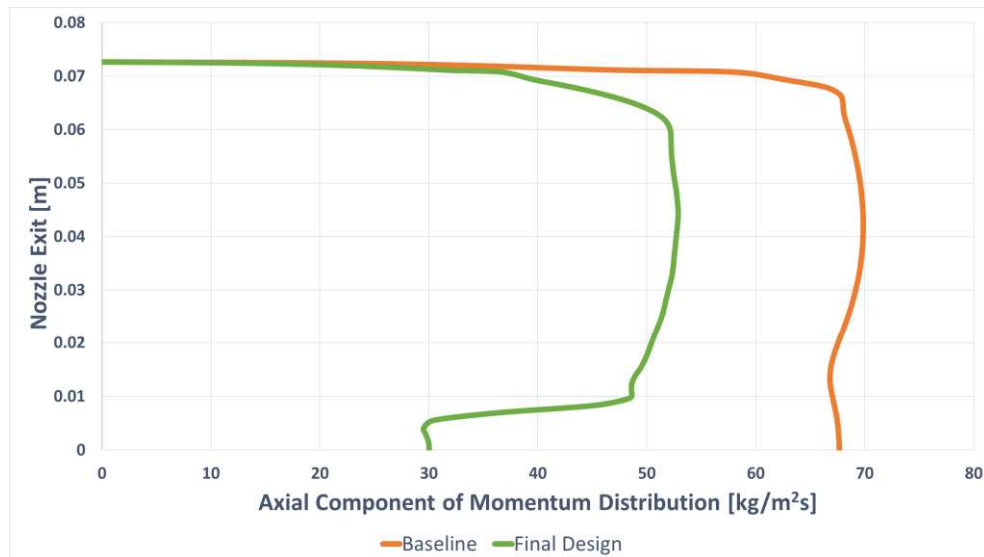
Figure 3.22. Distribution of Axial Component of Momentum at the Exit

From the distribution of axial component of momentum at the nozzle exit for baseline design and final design it is seen that discontinuity hugely affects the momentum distribution through the exit section too. Also, axial component of momentum is highly decreased when the Mach number is increased. In addition, ρu^2 distribution along the exit is represented.

a

b
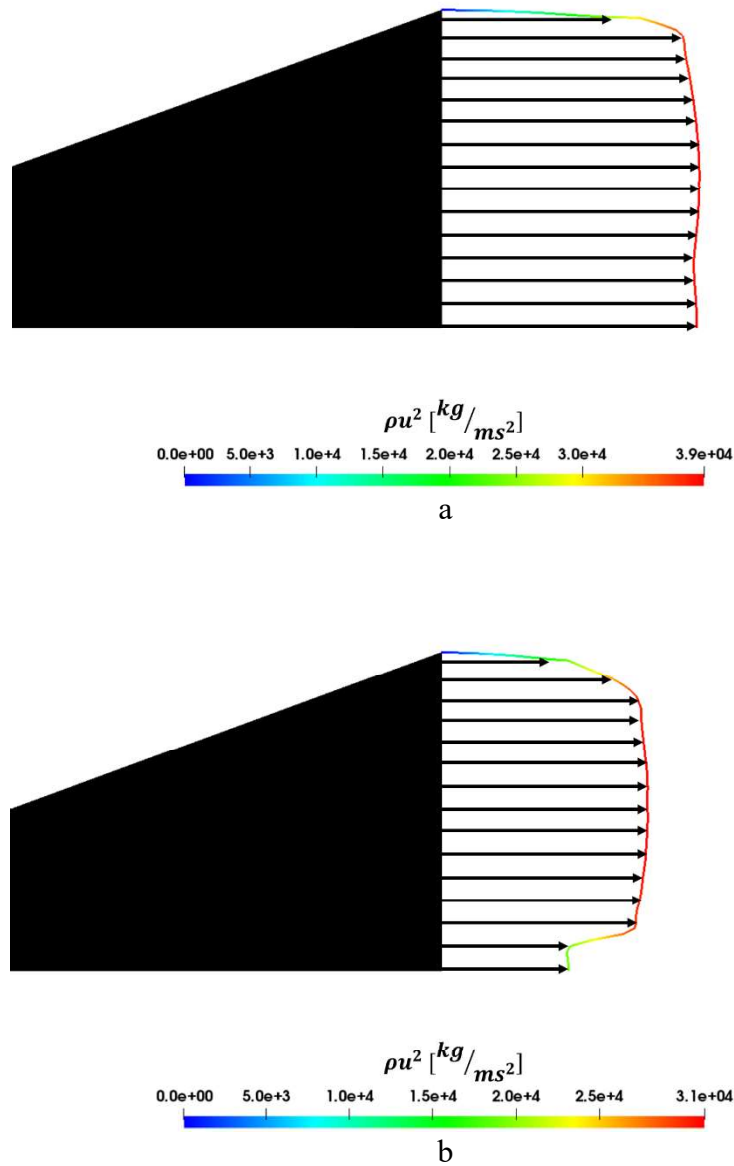
Figure 3.23. ρu^2 Distribution at the Exit a) Baseline b) Final Design

Since the ρu^2 distribution is directly related with the net thrust generated the distribution of it is represented in Figure 3.23. It is seen that ρu^2 along the nozzle exit is decreased in final design with respect to the baseline.

To conclude this study the observation is that; although a discontinuity generated, this optimization process successfully achieves its objective. Average Mach number at the exit section is increased 11.72 %. One must note that the pressure accordingly the density of the exit section drops. Therefore, the net thrust generated is decreased by 23.0 %.

3.2.2. Shape Optimization of Throat & Diverging Section Profile

After discontinuity problem in the throat deformation study is condsidered, design area is expanded from throat to the divergent section. Therefore, FFD boxes are created such that they enclose throat and the diverging section of the supersonic converging diverging nozzle.

In order to choose the most effective one, 3 different FFD boxes are created through the nozzle profile. All of them encloses both throat and diverging section. The starting and ending points of these FFD boxes are the same with each other. Starting points are not included to the deformation. Therefore, the first FFD box consists of 5 control points, the second one consists of 10 control points, the third and the last one consits of 15 control points. The number of control points equals to the design variables of an optimization study. Accordingly, changing the number of control points causes a change in the result of an optimization study. Since the result of the optimization study depends of the number of control points, these FFD boxes are subjected to an optimization procedure in order to see their effects on the objective function. The generated FFD boxes are represented in Figure 3.24.

a   b
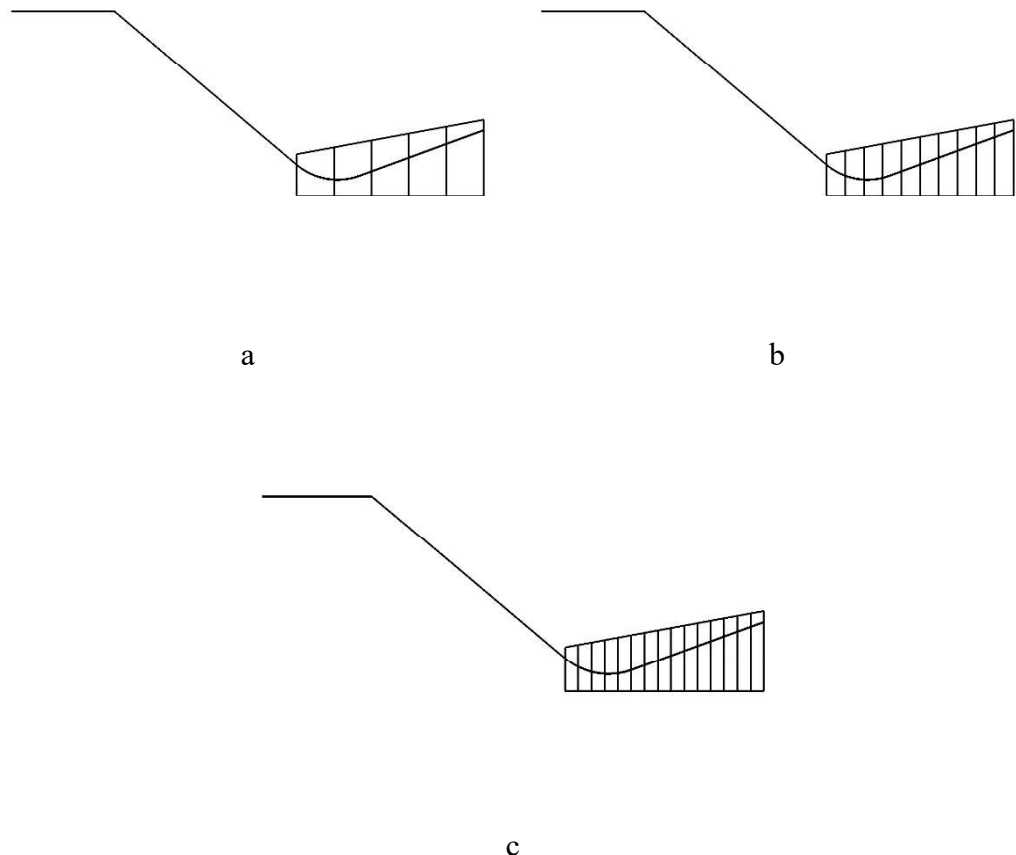
c
Figure 3.24. FFD Boxes Encapsulating Throat and Diverging Section a) 5 Control Points b) 10 Control Points c) 15 Control Points

Even though FFD boxes start from the converging section of the nozzle, since the flow there is subsonic possibility to have a discontinuity along the converging part diminishes. To see their effect on an objective function all of them are subjected to the Mach number maximization procedure. The deformation steps of all control points are kept constant and the same for each FFD box cases.

3.2.2.1. FFD Box Study and Mach Number Maximization

Different from the previous Mach number optimization case, in this part the geometry deformation spreads up to exit section of the supersonic converging diverging nozzle. To demonstrate the geometry change at the end of optimization

process, baseline geometries and the final designs are illustrated in the same frame for each FFD box cases.
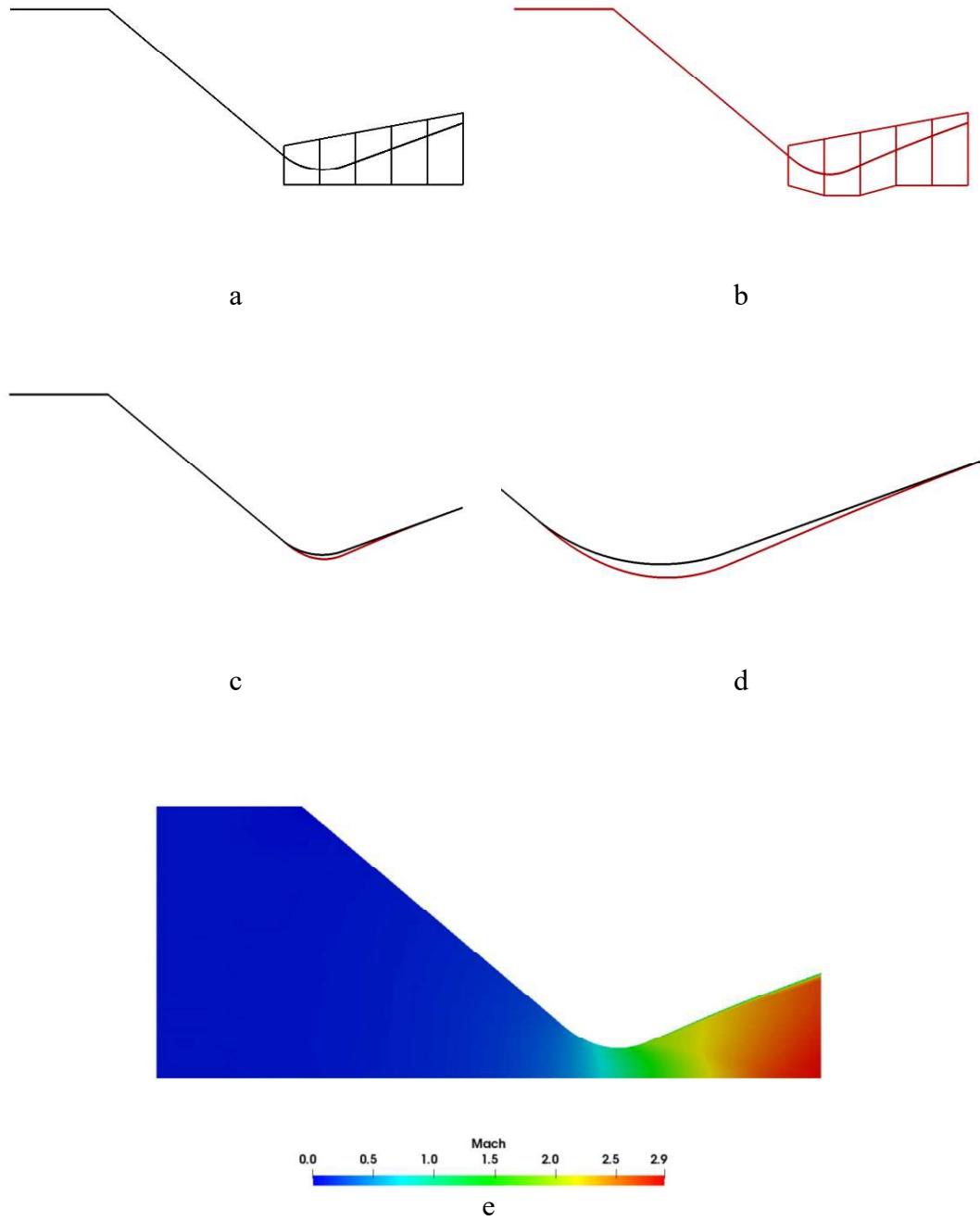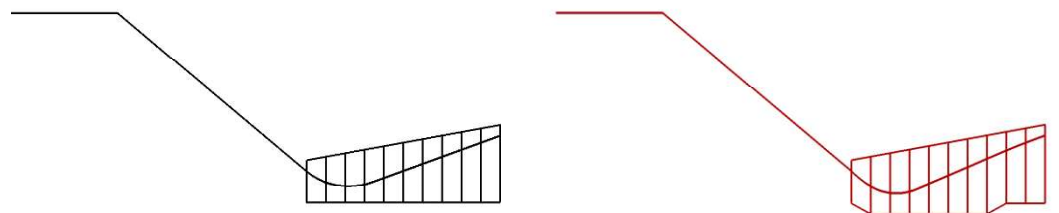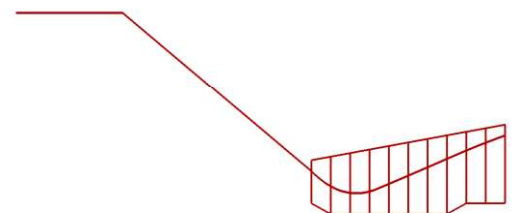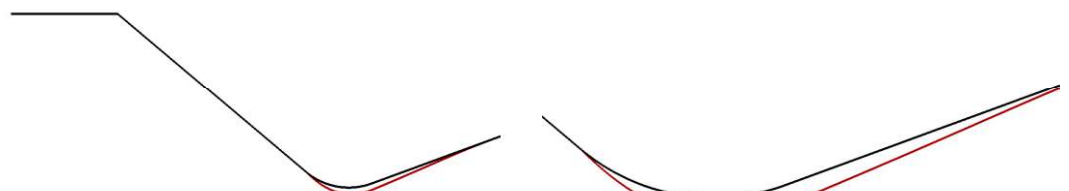
Figure 3.25. a) Baseline Geometry and Undeformed FFD Box b) Final Geometry and Deformed FFD Box c) Baseline and Final Geometry d) Baseline and Final Geometry Throat Profile e) Mach Number Contour of Final Design (5 Control Points)

a

b

c

d

e
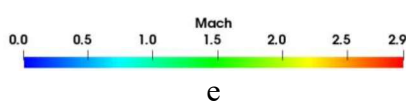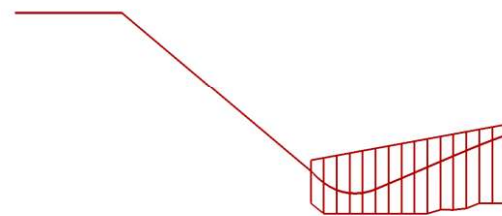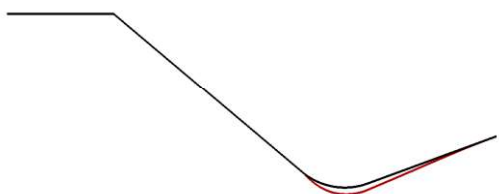
Figure 3.26. a) Baseline Geometry and Undeformed FFD Box b) Final Geometry and Deformed FFD Box c) Baseline and Final Geometry d) Baseline and Final Geometry Throat Profile e) Mach Number Contour of Final Design (10 Control Points)

51
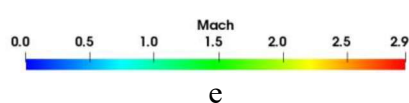
Figure 3.27. a) Baseline Geometry and Undeformed FFD Box b) Final Geometry and Deformed FFD Box c) Baseline and Final Geometry d) Baseline and Final Geometry Throat Profile e) Mach Number Contour of Final Design (15 Control Points)

The deformations and Mach number contours of all FFD box cases are represented in Figure 3.25, Figure 3.26 and Figure 3.27 respectively in an ascending order. In addition, average Mach number through the exit section is tabulated in Table 4.

Table 4. Exit Mach Numbers of Baseline Geometry and Final Designs of FFD Box Cases

Design	FFD Box Control Points	Exit Mach Number
Baseline Geometry	-	2.560
Final Design	5	2.757
Final Design	10	2.860
Final Design	15	2.865

As it can be seen from the Table 4, average Mach number values achieved by 10 and 15 control points are close to each other. The increase in objective function with respect to baseline geometry is, 7.70 % for 5 control points, 11.72 % for 10 control points 11.91 % for 15 control points.

From the Mach number contours it is seen that the flow expands smoothly without any discontinuity through the flow field. Also, Mach number profiles at the exit surface of baseline design and final designs for all the FFD boxes are represented in Figure 3.28. This figure clearly shows that Mach number at the exit increases after optimization procedure, and unlike the previous one, the uniformity is not damaged in this time Therefore, it is proven that the expansion of FFD boxes through the diverging section approach successfully manages the optimization procedure.
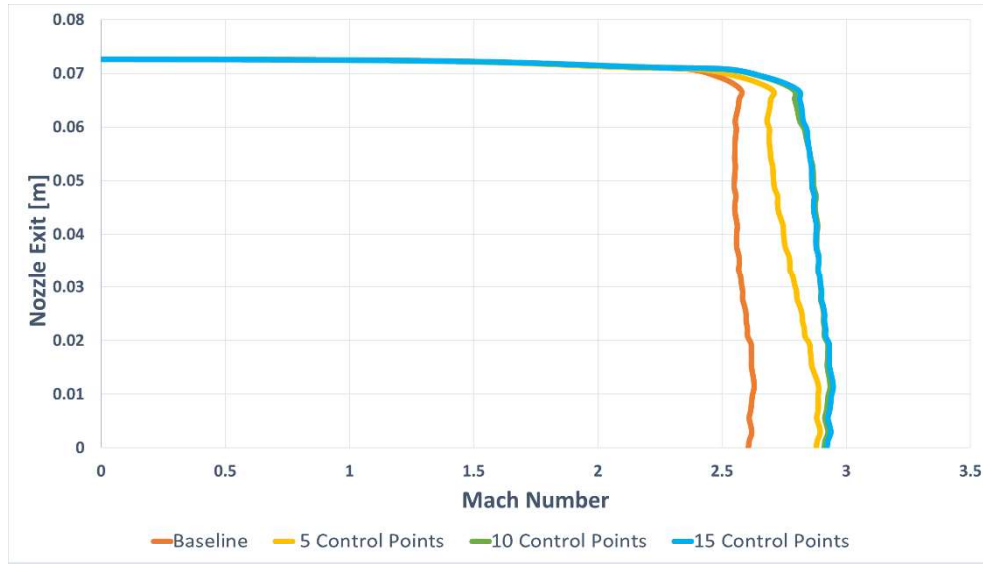
Figure 3.28. Mach Number Variations at the Exit

From Figure 3.28, it is seen that maximum Mach number is close to each other for 10 control points and 15 control points cases. However, 15 control points has achieved slightly higher values than the final design of 10 control points.

In order to choose the most effective FFD box, the variation of objective function with respect to the optimization iterations are plotted in Figure 3.29. As it can be understood from Figure 3.29 it takes 24 optimization iterations to converge 11.72 % increase in objective function for 10 control points case. On contrary, it takes 70 iterations to converge 11 91 % increase for 15 control points case. Therefore, the difference between their increments in objective function is small and there is huge difference in the number of iterations FFD box with 10 control points case is chosen for the rest of the study.

Since its effectiveness is proven, 10 control points case is chosen for the oncoming optimization studies. To see the result of chosen FFD box in terms of axial component of momentum, the distribution at the exit section is represented for baseline and the final design in Figure 3.30.
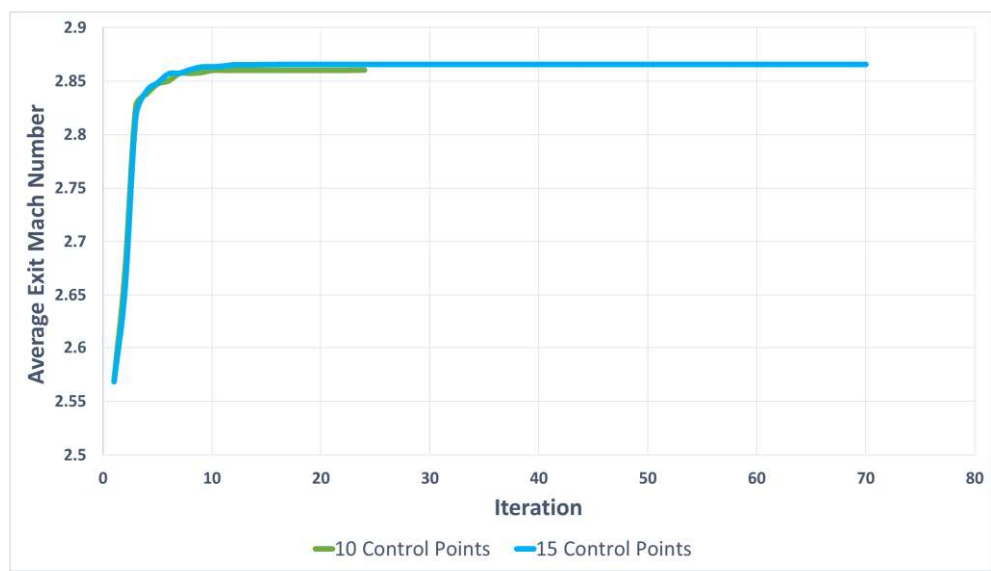
Figure 3.29. Change in Objective Function with Iterations
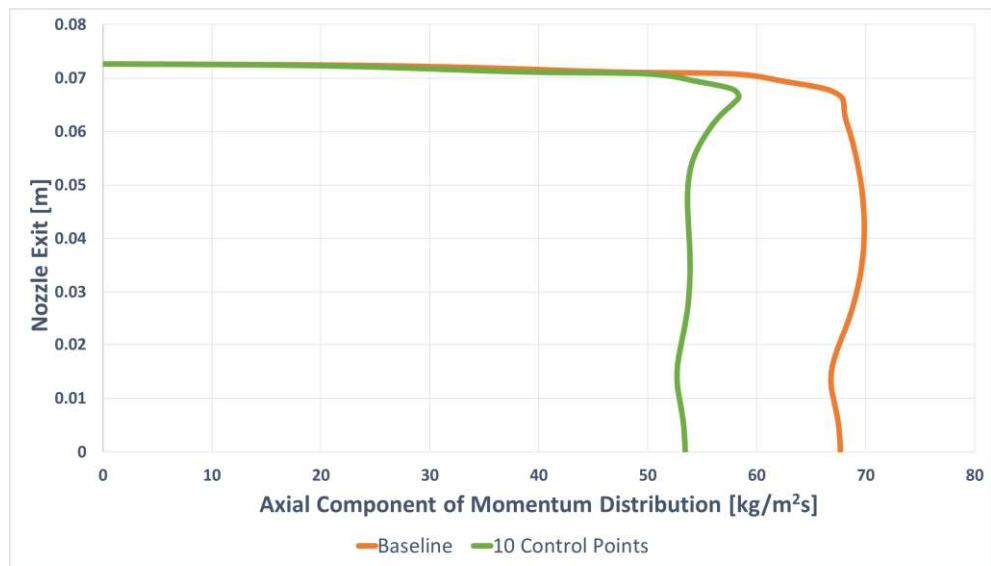
Figure 3.30. Distribution of Axial Component of Momentum at the Exit

Figure 3.30 shows that while the flow is accelerated the axial component of the momentum is decreased.
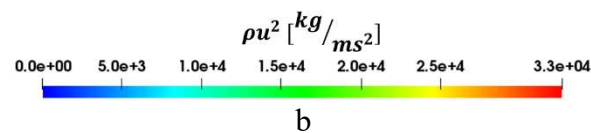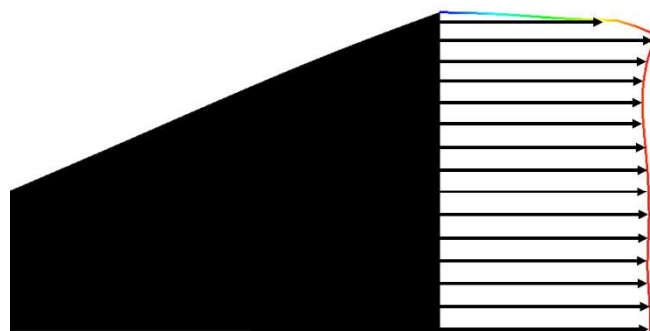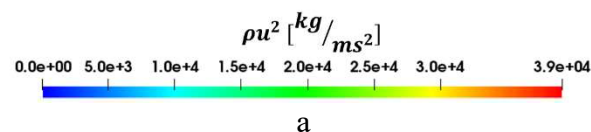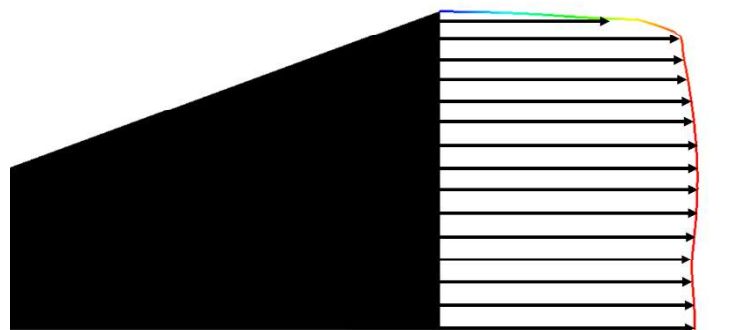
Figure 3.31. ρu^2 Distribution at the Exit a) Baseline b) Final Design (10 Control Points)

As mentioned, axial component of the momentum is decreased at the end of Mach number maximization study. To see its effect on the generated net thrust, ρu^2 distribution along the exit section is also represented. Figure 3.31 shows that the ρu^2 values are also decreased at the exit section.

From this study, it can be clearly seen that Mach number of the all optimization processes are increased with respect to the baseline design. The optimizer has successfully designed a new profile by lowering the throat value. Accordingly, it manages to obtain higher Mach number at the exit section. The increases in Mach number results in decrease in the net thrust generated due to drop in pressure and density accordingly. The net thrust of final design obtained from FFD box having 10 control points drops 17.65 %.

3.2.2.2. Mass Flow Rate Maximization

As well as Mach number, mass flow rate is also a parameter that affects thrust of a supersonic converging diverging nozzle. For the purpose of having optimum thrust mass flow rate must be increased. Baseline geometries throat and diverging section is enclosed by the same free form deformation box with 10 control points to have proper shape deformation.

It is expected that as a result of the optimization study, baseline geometry is deformed such that the final geometry has higher throat area. The results of the optimization study are given in Figure 3.32. In that figure, baseline nozzle profile with undeformed FFD box, final design nozzle profile with deformed FFD box and comparison of baseline and final design in terms of their profile are represented. Also, the objective function values are tabulated in Table 5 for the baseline and final design.

a   b

c   d
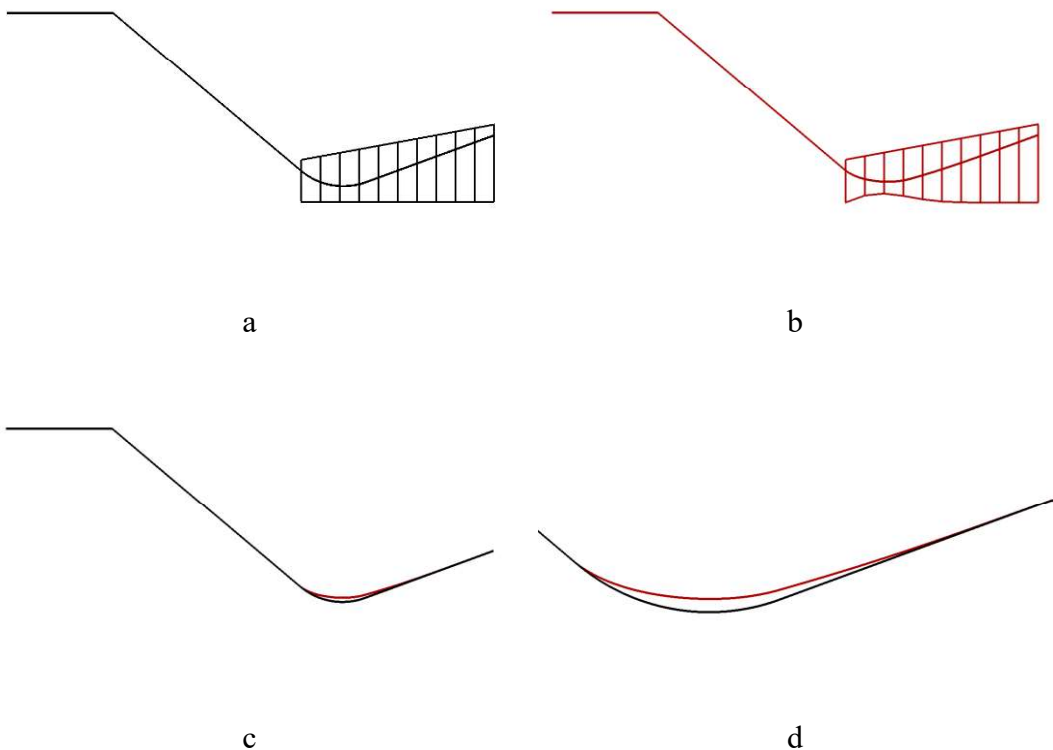
Figure 3.32. a) Baseline Geometry and Undeformed FFD Box b) Final Geometry and Deformed FFD Box c) Baseline and Final Geometry d) Baseline and Final Geometry Throat Profile

Table 5. Normalized Mass Flow Rate of Baseline Geometry and Final Design

Design	Normalized Mass Flow Rate
Baseline Geometry	1.0
Final Design	1.12

It must be noted that mass flow rate of the final design increased 12.0 % with respect to the baseline design. This is because the optimizer manages to obtain higher mass flow rate at the exit section by increasing the throat area. In order to see whether a discontinuity exists through the flow field Mach number contour of final design is

represented in Figure 3.33. To have a comparison Mach number contour of baseline is also represented in the same figure.

a

b

Figure 3.33. a) Mach Number Distribution of Baseline b) Mach Number Distribution of Final Design

From the Mach number contour it is seen that the flow expands smoothly without any discontinuity through the flow field for the final design. However, the Mach number at the exit of the nozzle is lower than the Mach number of the baseline design. This is because the throat area increases so that the expansion ratio of the nozzle decreases.

To compare the uniformity at the exit section Mach number variations of baseline and the final design are plotted in Figure 3.34. The effect of optimization on axial component of momentum is represented in Figure 3.35.
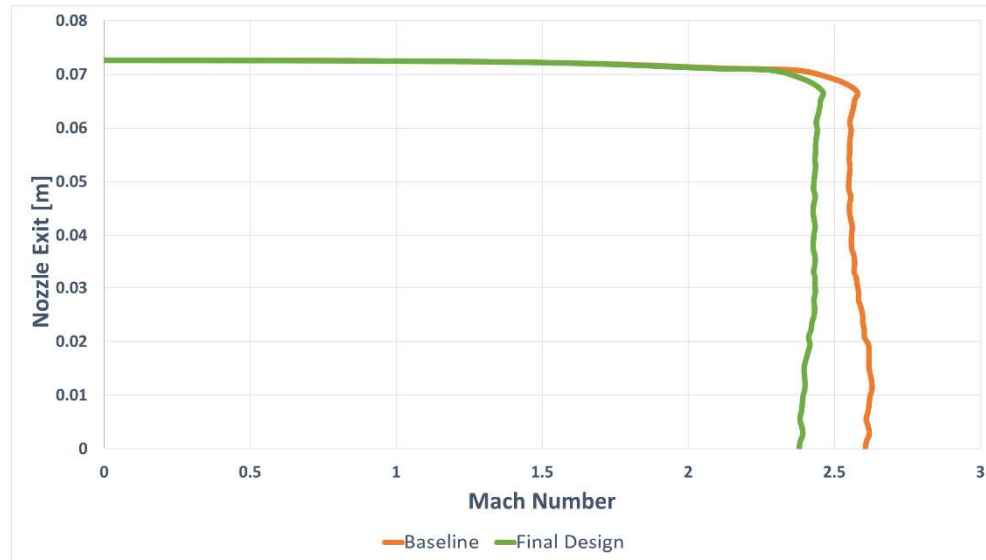
Figure 3.34. Mach Number Variation at the Exit
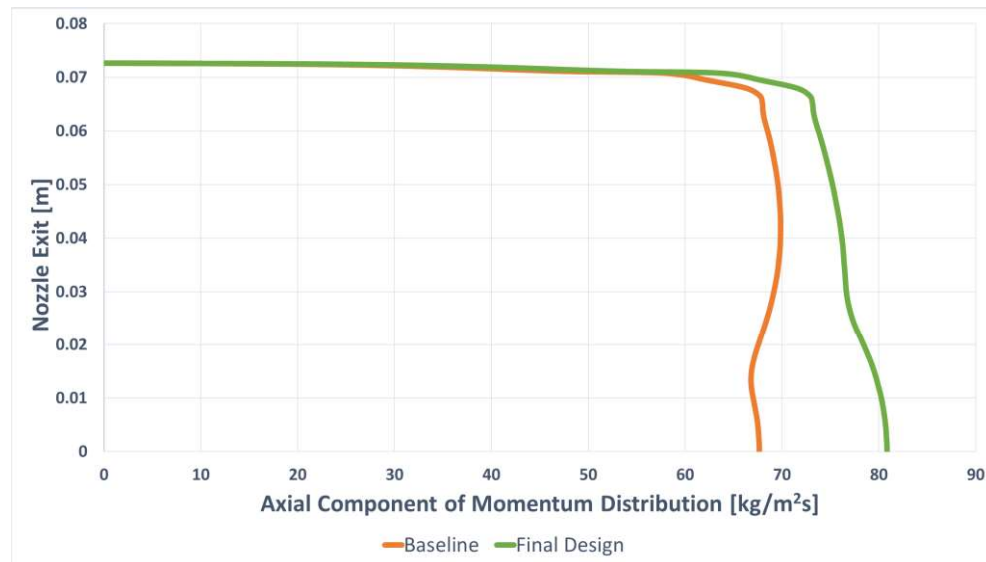
Figure 3.35. Distribution of Axial Component of Momentum at the Exit

As it can be seen from Figure 3.34; although the average Mach number is decreased at the exit section final design has more uniform flow compared to the baseline design and Figure 3.35 shows that momentum increases with higher mass flow rate.

$\rho u^2 \left[^{kg}/_{ms^2}\right]$

0.0e+00 5.0e+3 1.0e+4 1.5e+4 2.0e+4 2.5e+4 3.0e+4 3.9e+04

a

$\rho u^2 \left[^{kg}/_{ms^2}\right]$

0.0e+00 5.0e+3 1.0e+4 1.5e+4 2.0e+4 2.5e+4 3.0e+4 3.5e+4 4.4e+04

b
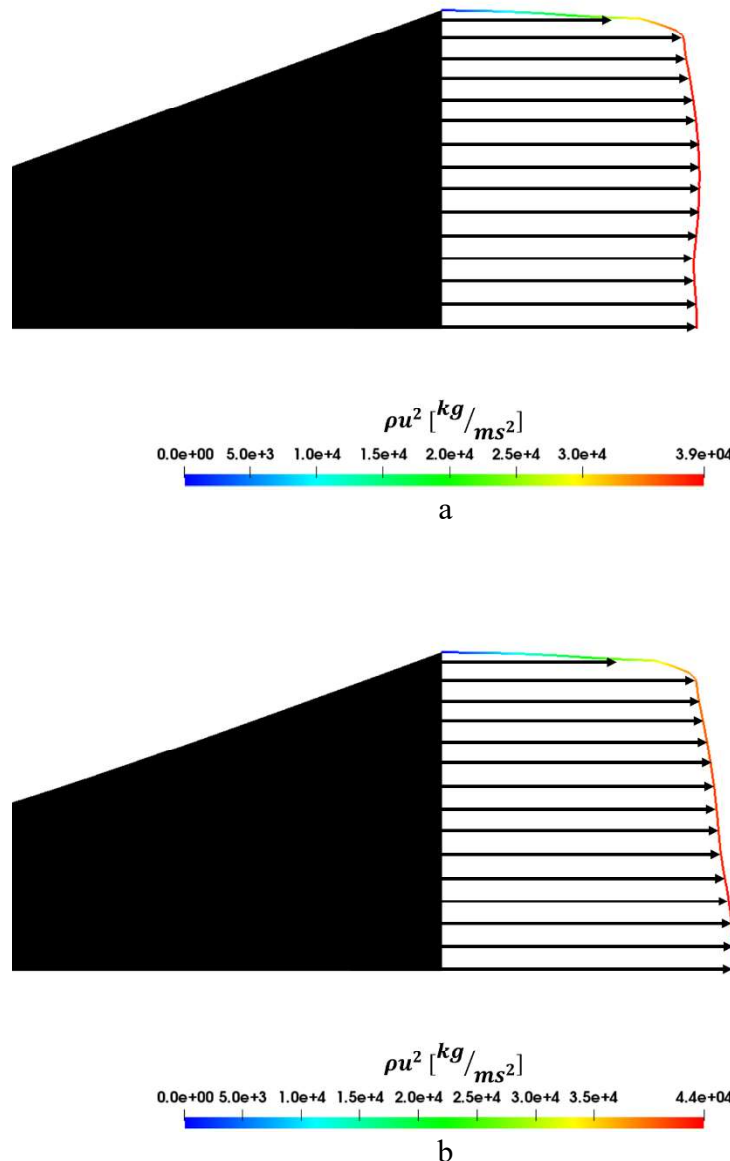
Figure 3.36. ρu^2 Distribution at the Exit a) Baseline b) Final Design

To see the effect of mass flow rate maximization on the generated net thrust, ρu^2 distribution along the exit section is also represented in Figure 3.36. As expected,

like the axial component of the momentum, ρu^2 values at the exit section are increased on the exit section of final design with respect to baseline. Thus, 8.88% increase in thrust is achieved at the end of mass flow rate maximization study.

3.2.2.3. Multi Objective Optimization

In the previous studies Mach number and mass flow rate parameters are subjected to optimization separately. For this study, both Mach number and mass flow rate are assigned into a multi objective optimization. The reason behind this to see if there is a change in the thrust value when these variables are tuned to obtain higher thrust in case, they are combined with each other. Together with the previous optimization work in this case same free form deformation box is used. Also, equal weight is given to these two parameters during the optimization study. Deformation steps of all control points are the same with each other for this study.

Along with the baseline geometry final design is illustrated on the same figure. The results of optimization studies are given in Figure 3.37 and in terms of shape deformation. This means the figure contains baseline nozzle profile with undeformed FFD box, final design nozzle profile with deformed FFD box and comparison of baseline and final design in terms of their profile. Also, the objective function values are tabulated in Table 6 . Normalized mass flow rate through the nozzle and average exit Mach number of it are tabulated in this table.

As it can be seen from the schematics of Figure 3.37, final design hugely differs from the baseline geometry especially at the throat section for multi objective optimization case. Therefore, the mass flow rate and the Mach number with respect to the baseline geometry is glaring. As tabulated in Table 6, average exit Mach number is dropped by 12.5 % while the Mass flow rate is increased 26.0 %.

<div align="center">a   b</div>

<div align="center">c   d</div>
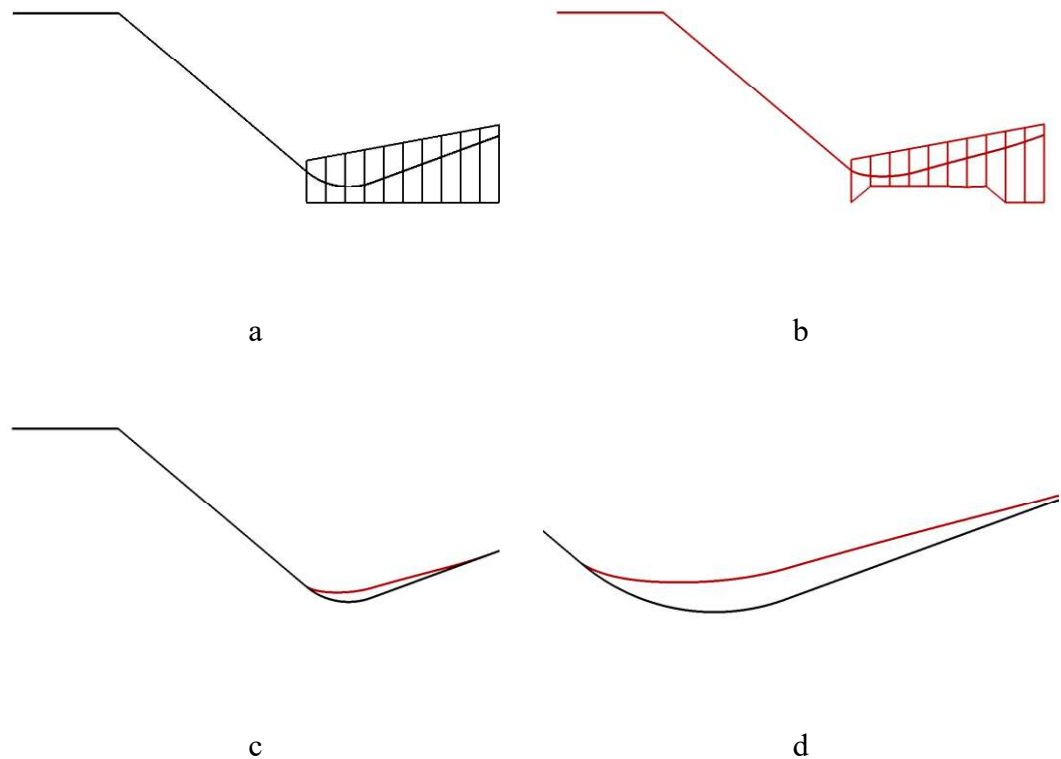
Figure 3.37. a) Baseline Geometry and Undeformed FFD Box b) Final Geometry and Deformed FFD Box c) Baseline and Final Geometry d) Baseline and Final Geometry Throat Profile

Table 6. Mach Number and Normalized Mass Flow Rate of Baseline Geometry and Final Design

Design	Mach Number	Normalized Mass Flow Rate
Baseline Geometry	2.56	1.0
Final Design	2.24	1.26

To see the flow fields, Mach number contours of baseline and final design are also represented in Figure 3.38.
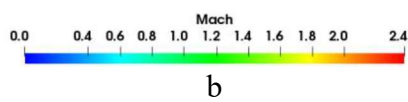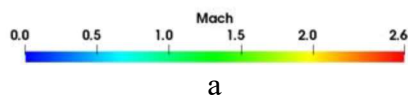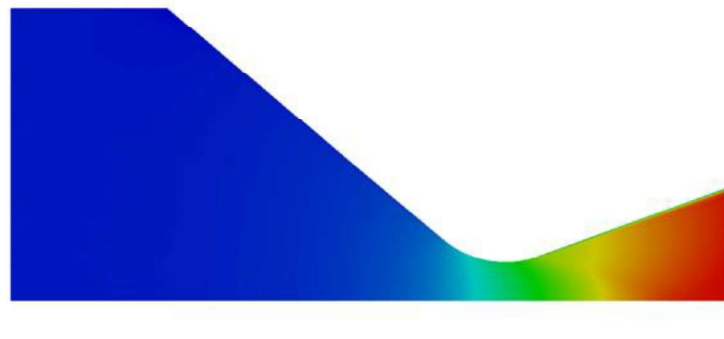
Figure 3.38. a) Mach Number Distribution of Baseline b) Mach Number Distribution of Final Design

Since the throat area increases the nozzle expansion ratio decreases. Therefore, maximum achieved Mach number is lower than the baseline design for the final design solution. Although the throat area changed much more than the previous studies, there is no discontinuity observed in the flow field. The changes in the Mach number along the exit line and the axial component of the momentum are given in Figure 3.39 and Figure 3.40.
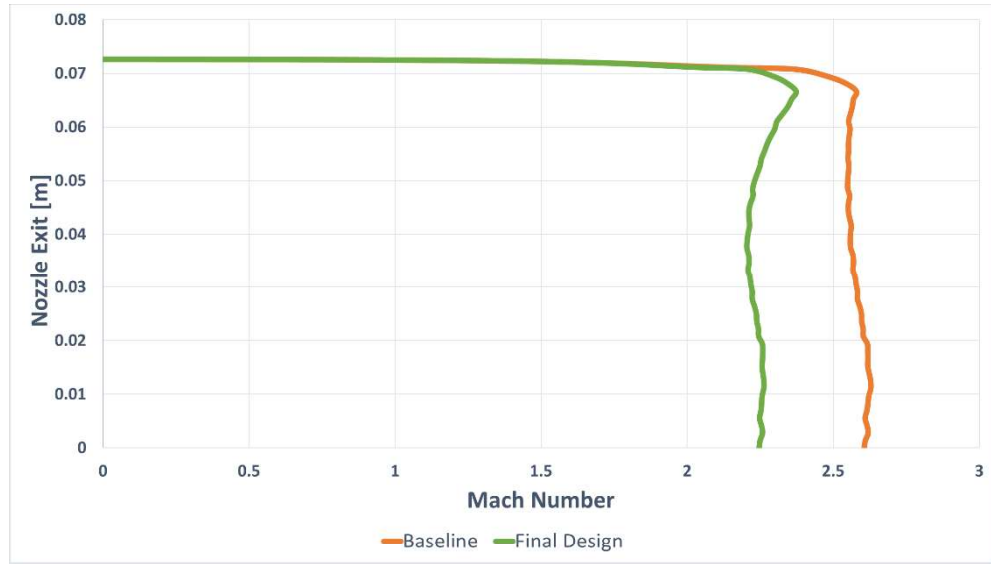
Figure 3.39. Mach Number Variation at the Exit
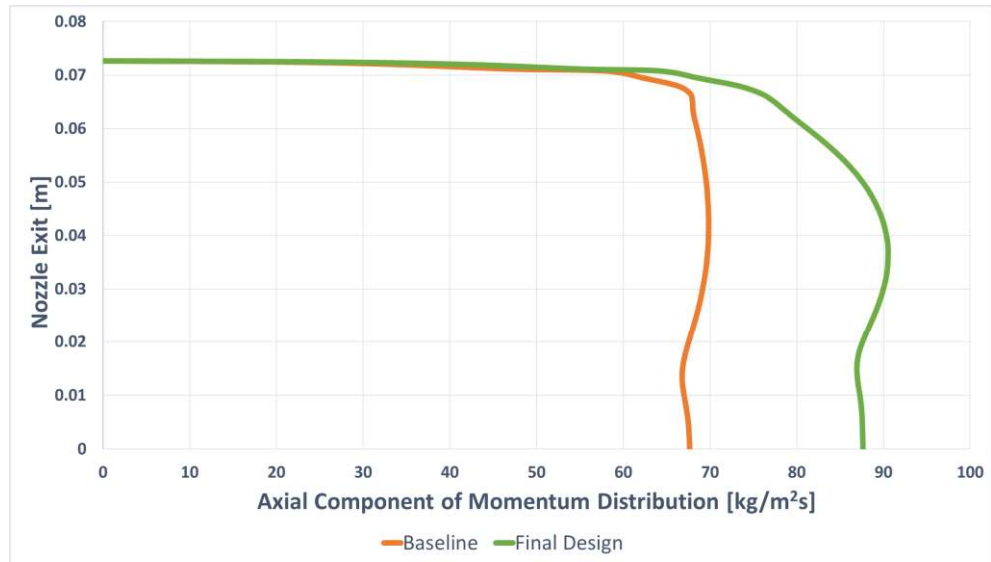
Figure 3.40. Distribution of Axial Component of Momentum at the Exit

Figure 3.39 and Figure 3.40 show that Mach number at the exit is decreased at the exit while the axial component of momentum is increased with respect to the baseline design. Thrust is calculated by using ρu^2 integrals on the exit surface. In

order to obtain information about change in thrust, the variation of ρu^2 at the exit surface is illustrated in Figure 3.41 for baseline and final design.
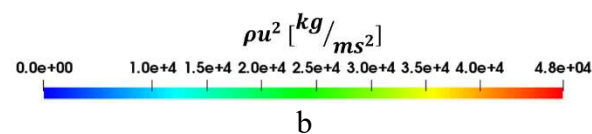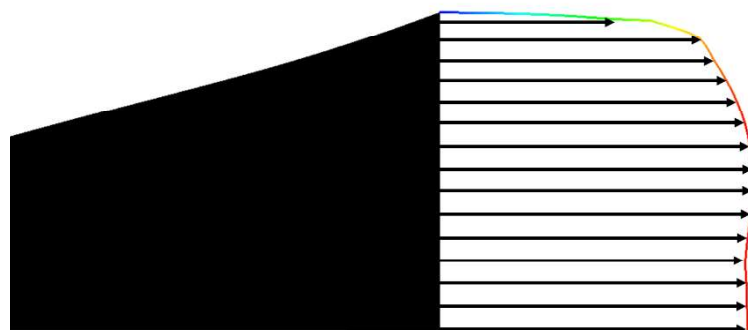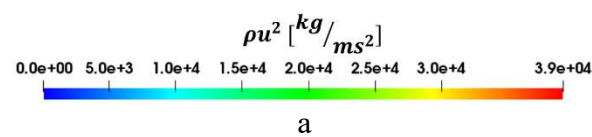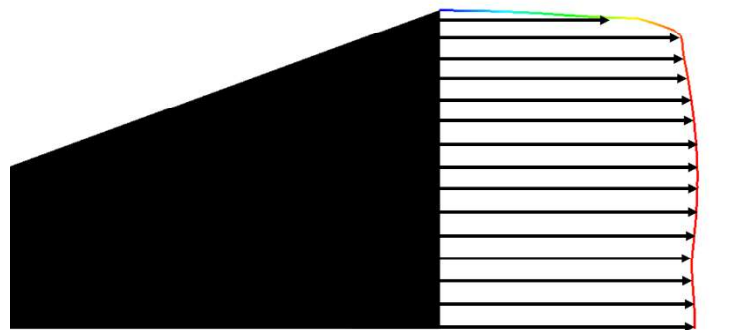
Figure 3.41. ρu^2 Distribution at the Exit a) Baseline b) Final Design

From Figure 3.41 it is seen that ρu^2 values at the nozzle exit are increased. Accordingly, the net thrust is increased by 19.04% at the end of multi objective optimization study. However, there is a strong drop 7.15 % drop in the total pressure is observed on the exit section of the nozzle is observed even though there is no strong discontinuity through the flow field. Therefore, a total pressure constraint must be assigned in order to have optimum thrust with efficient nozzle design.

3.2.2.4. Multi Objective Optimization with Total Pressure Constraint

During the multi objective optimization, it is seen that total pressure at the exit of the nozzle is dropped while the mass flow rate is increased extremely. This means that optimizer ignores the total pressure recovery while generating an enormous change in the mass flow rate and Mach number. Therefore, a constraint on total pressure at the exit section of the nozzle is assigned in addition to the multi objective optimization study. For this study, 1.5% total pressure drop with respect to the baseline design is designated as the constraint.

It is expected that as a result of the optimization study, baseline geometry is deformed such that the final geometry has higher throat area with smoother transitions in order not to have high total pressure drop. The results of the optimization study are given in Figure 3.42. The figure consists of baseline nozzle profile with undeformed FFD box, final design nozzle profile with deformed FFD box and comparison of baseline and final design in terms of their profile are represented. Also, the objective function values and the constraint value of baseline and final design are tabulated in Table 7 for the baseline and final design.

Figure 3.42 shows that the profile of the final design is disturbed towards to increase throat area but not as much as the unconstraint optimization case. Therefore, as shown in Table 7, Mach number at the exit section is decreased 1.56 %, mass flow rate of is increased 4.0 % and total pressure at the exit section is decreased 1.0 % for the final design with respect to the final design.

a   b

c   d
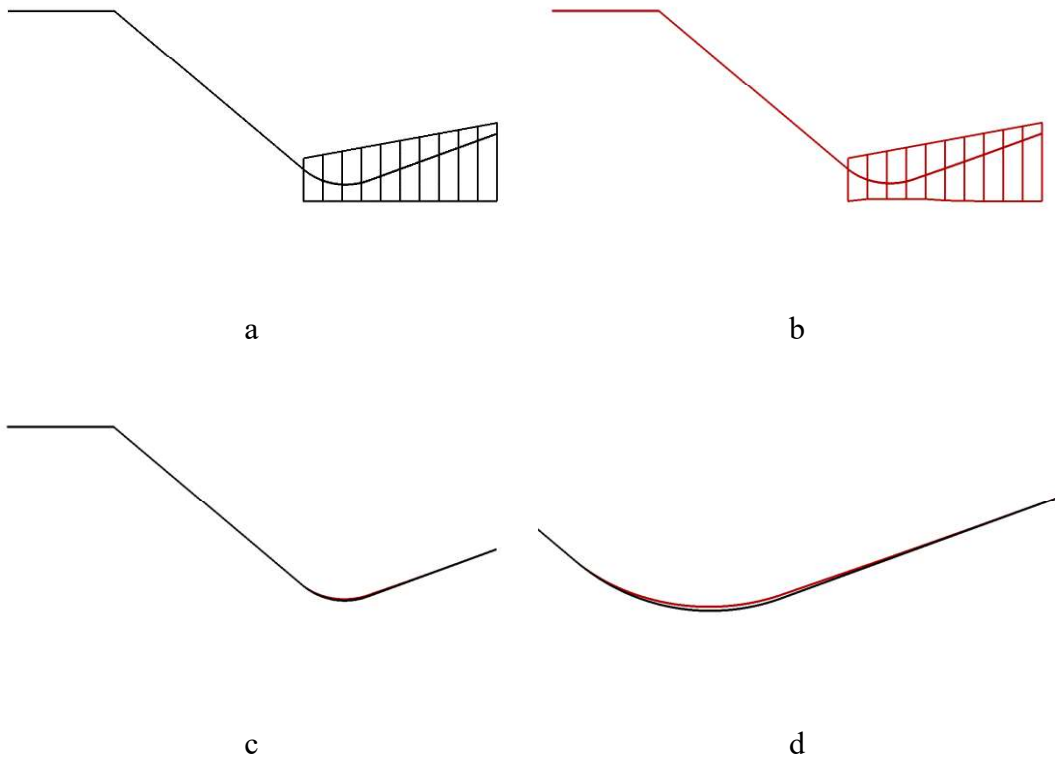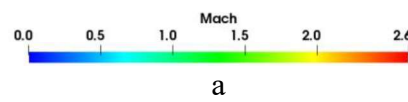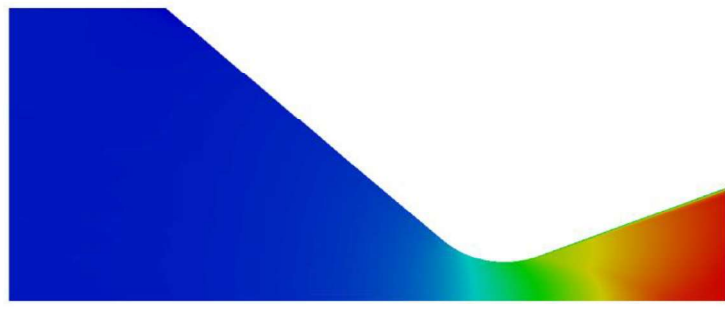
Figure 3.42. a) Baseline Geometry and Undeformed FFD Box b) Final Geometry and
Deformed FFD Box c) Baseline and Final Geometry d) Baseline and Final Geometry Throat
Profile
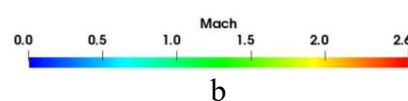
Table 7. Mach Number, Normalized Mass Flow Rate and Normalized Total Pressure of
Baseline Geometry and Final Design

Design	Mach Number	Normalized Mass Flow Rate	Normalized Total Pressure
Baseline Geometry	2.56	1.0	1.0
Final Design	2.52	1.04	0.99

In order to see the flow fields, Mach number contours of baseline and final design
are also represented in Figure 3.43. The figure shows that there is not an enormous
change in the flow field with the modification along the nozzle profile.

a

b

Figure 3.43. a) Mach Number Distribution of Baseline b) Mach Number Distribution of Final Design

The changes in the Mach number along the exit line and the axial component of the momentum are given in Figure 3.44 and Figure 3.45. These figures show that although Mach number at the exit section slightly decreases, the axial component of the momentum is increased.
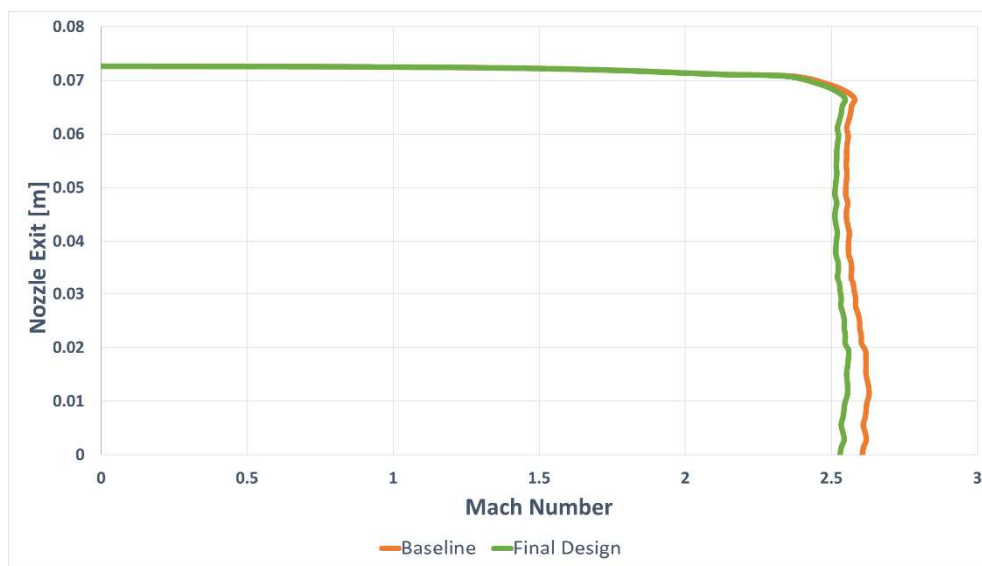
Figure 3.44. Mach Number Variation at the Exit
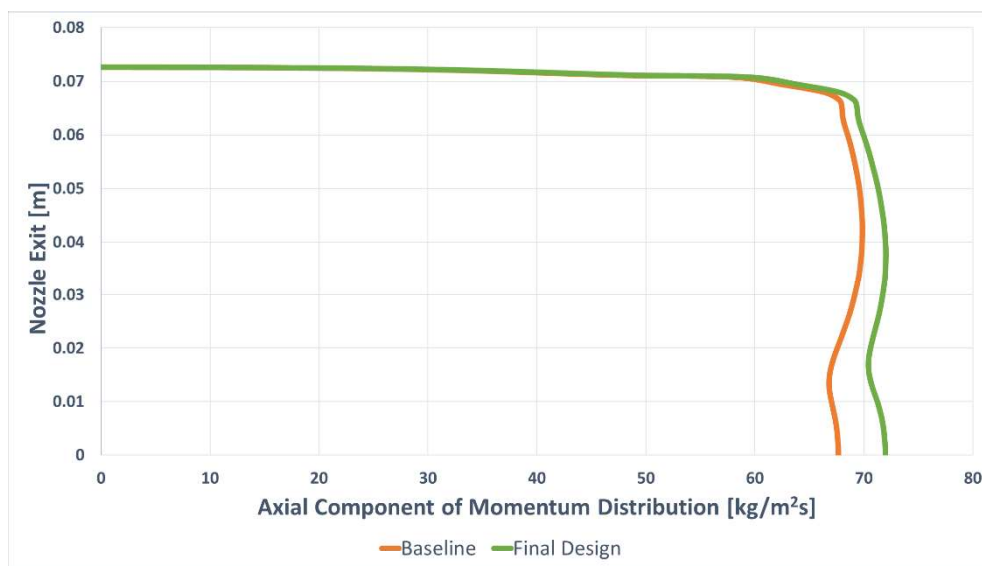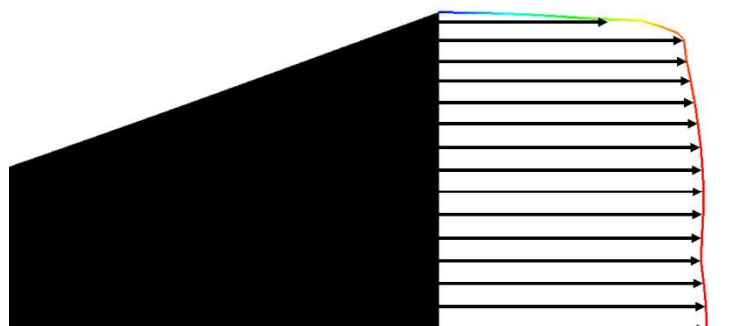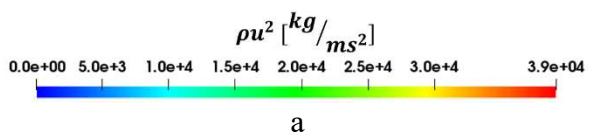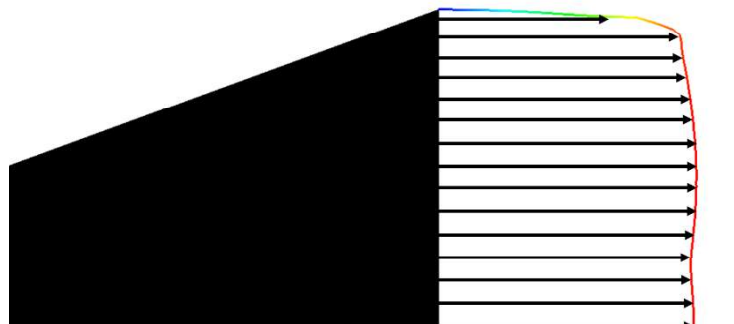
Figure 3.45. Distribution of Axial Component of Momentum at the Exit

In order to see the effects of these changes onto the net thrust, ρu^2 variations at the exit surfaces of baseline and final design are illustrated in Figure 3.46.

$$\rho u^2 \, [^{kg}/_{ms^2}]$$

0.0e+00   5.0e+3   1.0e+4   1.5e+4   2.0e+4   2.5e+4   3.0e+4   3.9e+04

a

$$\rho u^2 \, [^{kg}/_{ms^2}]$$

0.0e+00   5.0e+3   1.0e+4   1.5e+4   2.0e+4   2.5e+4   3.0e+4   3.5e+4   4.1e+04

b

Figure 3.46. ρu^2 Distribution at the Exit a) Baseline b) Final Design

Figure 3.46 shows that ρu^2 values at the nozzle exit are increased for the final design with respect to the baseline. Accordingly, the net thrust is increased by 2.84 % at the end of multi objective optimization with total pressure constraint study and the total pressure is dropped by 1.0 % with respect to the baseline.

3.2.2.5. Summary

In the discrete adjoint-based optimization study of supersonic converging diverging nozzles Mach number and mass flow rate at the exit section are the design objectives. During the study they are chosen as design objective separately, together and together with total pressure constraint. From the work it is observed that:

- Increase in exit Mach number decreases the mass flow rate and thrust.

- Increase in mass flow rate decreases exit Mach number but increases thrust.

- Multi objective optimization of both gives the best result in terms of thrust but decreases total pressure at the exit of the nozzle.

- Multi objective optimization of both with total pressure constraint successfully manages the maximize thrust without violating the assigned constraint value.

Change in thrust with the optimization iteration for unconstrained and constrained optimization studies is given in Figure 3.47.

Figure 3.47. Change in Normalized Thrust with Optimization Iteration

For the optimization studies the convergence criteria of objective function is chosen as 1.0×10^{-12} and the maximum iteration number is assigned as 100. As it can be seen in Figure 3.47, both studies are converged without reaching the maximum iteration number. While it takes 30 steps to have convergence during unconstrained optimization, constraint optimization reaches convergence in 27 steps.

Moreover, for the importance of choosing right boundaries for the FFD box in supersonic flow conditions is also noticed. During the throat section optimization, a discontinuity is observed at the end of the FFD box. The part that is deformed through the diverging section could not adjust itself to the nozzles remaining profile. Therefore, since the flow is supersonic there exists a shock wave inside of the designed nozzle.

During the verification procedure, it is observed that SST and SA turbulence models give similar results with respect to each other. However, SA turbulence model solution has pressure distributions of upper and lower divergent walls containing a drop towards to the end of the nozzle. Therefore, the SST turbulence model is subjected to the optimization procedure.

To summarize the whole work done by discrete adjoint based optimization using SU^2 is represented. From the table it is clearly seen that multi objective optimization gives better result for in terms of thrust however it is inefficient in terms of total pressure recovery. Therefore, total pressure constraint is assigned to the multi objective optimization study and the optimizer successfully manages to accomplish the constraint. All the optimization studies are summarized in Table 8.

Table 8. Optimization Summary

FFD Box	Assigned Objective Function / Constraint	Change in the Objective Function / Constraint	Change in the Net Thrust
Throat	Exit Mach Number / No Constraint	11.72 % Increase	23.0 % Decrease
Throat & Diverging Section	Exit Mach Number / No Constraint	11.72 % Increase	17.65 % Decrease
Throat & Diverging Section	Mass Flow Rate / No Constraint	12.0 % Increase	8.88 % Increase
Throat & Diverging Section	Exit Mach and Mass Flow Rate Multi Objective / No Constraint	12.5 % Decrease in Exit Mach Number 26.0 % Increase in Mass Flow Rate	19.04 % Increase
Throat & Diverging Section	Exit Mach and Mass Flow Rate Multi Objective / Total Pressure Constraint	1.56 % Decrease in Exit Mach Number 4.0 % Increase in Mass Flow Rate / 1.0 % Decrease in Total Pressure (1.5 % Decrease Allowed)	2.84 % Increase

CHAPTER 4

CONCLUSIONS & FUTURE WORK

4.1. Conclusions

In this thesis, discrete adjoint based optimization of supersonic converging diverging nozzle by using open-source CFD tool SU^2 is investigated. During the work two different design objectives are used in order the optimize the thrust eventually. The first objective is flow Mach number at the exit section of the nozzle. In the investigation of Mach number study, it is seen that increasing Mach number decreases the mass flow rate and the net thrust generated by the nozzle. To increase the Mach number optimizer tries to decrease the nozzle throat area. However, this results in lower mass flow rate through the nozzle. The second objective is the mass flow rate though the nozzle. The optimizer tries to increase mass flow rate of the nozzle with higher throat area. Therefore, this results in lower Mach number at the exit section. On contrary to the first study, increase in mass flow rate results in increase of thrust even though the Mach number at the exit section is decreased. This is because the expansion through the nozzle is less than the baseline design so that it has higher density at the exit of the nozzle. Accordingly, since the density is increased the net momentum is increased. For the third study, Mach number and mass flow rate are both chosen as a design objective for the multi objective study. Therefore, net thrust at the end of the study is the highest value achieved. However, total pressure at the exit of the nozzle is dropped with down with high percentage. Therefore, as a final study a total pressure constraint is assigned to the multi objective study in order to get acceptable pressure recovery. In this case, optimizer successfully manages to maximize the objective function without violating the constraint. The bright side of this optimization study is optimizer adjusts the design procedure to have mass flow rate without destructing the supersonic outflow and

total pressure recovery. Therefore, the balance between mass flow rate, exit Mach number and the total pressure is established.

4.2. Future Work

This study contains discrete adjoint based optimization of a supersonic converging diverging nozzle. As a future work; firstly, continuous adjoint based optimization can be tried. Therefore, advantages and disadvantages of continuous adjoint approach can be observed. Secondly, there can be three-dimensional optimization of supersonic converging diverging nozzle. With this way three-dimensional wall effects will be included to the optimization.

REFERENCES

[1]   R. D. Flack, *Fundamentals of jet propulsion with applications*, vol. 17. Cambridge University Press, 2005.

[2]   G. P. Sutton and O. Biblarz, "Rocket Propulsion Elements Seventh Edition," 2001.

[3]   M. Prathibha, M. S. Gupta, and S. Naidu, "CFD Analysis on a Different Advanced Rocket Nozzles," 2015.

[4]   J. D. Mattingly, "Elements of Gas Turbine Propulsion •."

[5]   T. D. Economon, F. Palacios, S. R. Copeland, T. W. Lukaczyk, and J. J. Alonso, "SU2: An Open-Source Suite for Multiphysics Simulation and Design," *AIAA J.*, 2015.

[6]   F. Palacios, T. D. Economon, and J. J. Alonso, "Stanford University Unstructured (SU2): An open-source integrated computational environment for ...," no. January 2013, 2014.

[7]   T. A. Albring, M. Sagebaum, and N. R. Gauger, "Development of a Consistent Discrete Adjoint Solver in an Evolving Aerodynamic Design Framework," in *16th AIAA/ISSMO Multidisciplinary Analysis and Optimization Conference*, 2015.

[8]   A. Jameson and J. Reuther, "Control Theory Based Airfoil Design Using the Euler Equations."

[9]   H. L. Rozendaal, "A generalized method for the design of optimum rocket nozzles."

[10]   S. J. -Professor B MOSS, "HADDAD SUPERSONIC NOZZLE DESIGN OF ARBITRARY CROSS-SECTION."

[11]   K. S. Patel, "Flow Analysis and Optimization of Supersonic Rocket Engine Nozzle at Various Divergent Angle using Computational Fluid Dynamics (CFD)."

[12]   A. S. Swaroopini, M. Ganesh Kumar, T. Naveen Kumar, and A. Professor, "NUMERICAL SIMULATION AND OPTIMIZATION OF HIGH PERFORMANCE SUPERSONIC NOZZLE AT DIFFERENT CONICAL ANGLES."

[13]   G. Caramia and A. Dadone, "A Discrete Adjoint Formulation for Inviscid Flow Nozzle Optimization," in *Energy Procedia*, 2017.

[14]   H. K. Versteeg *et al.*, "An Introduction to Computational Fluid Dynamits Second Edition."

[15]   T. Cebeci, "Turbulence models and their application: efficient numerical methods with computer programs," 2003.

[16]   *Closure Strategies for Turbulent and Transitional Flows*. 2010.

[17]   F. Menter, "Zonal Two Equation k-w Turbulence Models For Aerodynamic Flows," in *23rd Fluid Dynamics, Plasmadynamics, and Lasers Conference*, 1993.

[18] F. R. Menter, "Two-equation eddy-viscosity turbulence models for engineering applications," *AIAA J.*, 1994.

[19] T. W. Taylor, F. Palacios, K. Duraisamy, and J. J. Alonso, "A hybrid adjoint approach applied to turbulent flow simulations," 2013.

[20] F. Palacios *et al.*, "Stanford University Unstructured (SU^2): An open-source integrated computational environment for multi-physics simulation and design," 2013.

[21] A. JAMESON, W. SCHMIDT, and E. TURKEL, "Numerical solution of the Euler equations by finite volume methods using Runge Kutta time stepping schemes," in *14th Fluid and Plasma Dynamics Conference*, 1981.

[22] J. R. Shewchuk, "Lecture Notes on Delaunay Mesh Generation," 2012.

[23] G. Yang and A. Da Ronch, "Aerodynamic Shape Optimisation of Benchmark Problems Using SU2," 2018.

[24] T. A. Albring, M. Sagebaum, and N. R. Gauger, "Efficient Aerodynamic Design using the Discrete Adjoint Method in SU2," in *17th AIAA/ISSMO Multidisciplinary Analysis and Optimization Conference*, 2016.

[25] M. Biava, M. Woodgate, and G. N. Barakos, "Fully Implicit Discrete-Adjoint Methods for Rotorcraft Applications," *AIAA J.*, 2015.

[26] A. C. Duffy, "An Introduction to Gradient Computation by the Discrete Adjoint Method."

[27] M. B. Giles and N. A. Pierce, "An Introduction to the Adjoint Approach to Design," 2000.

[28] T. D. Economon, F. Palacios, and J. J. Alonso, "A Viscous Continuous Adjoint Approach for the Design of Rotating Engineering Applications," in *21st AIAA Computational Fluid Dynamics Conference*, 2013.

[29] T. D. Economon, J. J. Alonso, T. Albring, and N. R. Gauger, "Adjoint formulation investigations of benchmark aerodynamic design cases in SU2," in *35th AIAA Applied Aerodynamics Conference, 2017*, 2017.

[30] O. P. Kostić, Z. A. Stefanović, and I. A. Kostić, "CFD modeling of supersonic airflow generated by 2D nozzle with and without an obstacle at the exit section," *FME Trans.*, 2015.